出芽酵母の形態変化に基づく vanillin の細胞内標的探索

菅洋平

東京大学大学院
新領域創成科学研究科
先端生命科学専攻

２０１１年
修士論文

Exploring Cellular Targets of Vanillin Based on Morphological Changes of *Saccharomyces cerevisiae*

Yohei Suga

Department of Integrated Biosciences
Graduate School of Frontier Sciences
University of Tokyo

2011
Master Thesis

Table of Contents

List of Figures

List of Tables

Acknowledgments

I wish to express my deepest gratitude to an outstanding and experienced Geneticist, Prof. Yoshikazu Ohya for his supervision and advice throughout this study.

I am deeply grateful to Dr. Satoru Nogami for his helpful advice, discussion and encouragement.

I would like to thank Dr. Shinsuke Ohnuki and Dr. Takahiro Negishi for their statistical and technical support.

I would like to thank Seiko Morinaga for her technical support and advices.

I also thank all members of laboratory of signal transduction, Department of Integrated Biosciences Graduate School of Frontier Sciences, for their encouragement.

Last but not least, I also thank my family for mental and financial support.

Abbreviations

DMSO	dimethylsulfoxide
EUROSCARF	european *Saccharomyces cerevisiae* archive for functional analysis
FDR	false discovery rate
GO	gene ontology
PCA	principal component analysis
PCR	polymerase chain reaction
WT	wild-type
SCMD	*Saccharomyces cerevisiae* morphological database
SGD	Saccharomyces genome database
TRIS	tris (hydroxymethyl) aminomethane

Summary

Vanillin is one of the major phenolic compounds degraded from lignin. It is considered as a problematic byproduct of bioethanol production from lignocelluloses since it inhibits yeast growth and fermentation. However, detailed inhibitory mechanisms of vanillin are still unknown. In this study, I investigated intercellular targets of vanillin based on the image profiling method to infer the drug targets developed recently (Ohnuki *et al*., 2010). Using this method, I revealed that the morphology of wild-type cells treated with vanillin is similar with that of *erg6*Δ and *his3*Δ *adh6*Δ treated with vanillin. From the result of *erg6*Δ, the mutant of elgosterol-biosynthesis, it was suggested that vanillin does not affect its pathway. From the result of *his3*Δ *adh6*Δ, the mutant of vanillin-conversion, it was suggested that the accuracy of the image profiling was increased probably due to the inability of vanillin bio-conversion of *his3*Δ *adh6*Δ, which makes the effects of vanillin more aggravate. In common with the three strains, cell sizes were reduced in the presence of vanillin in a dose-dependent manner and significant enrichment of gene ontology term “ribosomal large subunit” was detected in the inference results. In conclusion, these results suggest that vanillin affects ribosome or related components in yeast cells and induces growth defect.

Introduction

Bioethanol is produced by the action of microorganisms and the enzymes through the fermentation of sugars, starches or cellulose. It has been attractive as an alternative to fossil fuel because of its depletion and the global warming. Bioethanol used today is mainly produced from sugar cane or corn starch (Parawire and Tekere, 2010), although these crude materials are also main food or feed resources. In order to produce sufficient bioethanol and to save food resources, it is necessary to use stover and corn residue for bioethanol production to conserve the corn kernel itself (NEDO: New Energy and Industrial Technology Development Organization, report NO.977, 2006). In that case, lignocellulosic biomass such as these residues and wood chips are very important crude materials for bioethanol (Hahn-Hägerda *et al*., 2006).

Lignocellulose composed of lignin, hemicelluloses and cellulose is the main substance of plant cell wall. To produce bioethanol from lignocellulosic materials, thermo-chemical pre-treatment is needed before the fermentation in order to break the rigid binding of cellulose and hemicelluloses with lignin (Pu *et al*., 2008). However, this process leads to the formation of the inhibitory compounds against fermentation, which can be put into three major groups; furaldehydes, weak acids and phenolics (Klinke *et al*., 2004). Vanillin (Figure 1) is one of the major phenolic compounds degraded from

lignin. Since vanillin inhibits yeast growth and fermentation, it is also considered as a problematic inhibitor for fermentation (Cantarella *et al*., 2004). Thus, it is very important to know the mode of action of vanillin which inhibits yeast growth, especially for the more efficient bioethanol production.

From other aspects, vanillin is a phenolic compound contained in the beans of *Vanilla* tree and used as a flavoring material all over the world. It is also chemically synthesized and an approximately 50% of the worldwide production of such vanillin is used as an intermediate product in chemical and pharmaceutical industries. For example, herbicides, antifoaming agents or drugs such as papaverine, L-dopa, L-methyldopa and the antimicrobial agent, trimethoprim are made from vanillin (Hocking, 1997). In common with other phenolic compounds, vanillin displays antioxidant property (Burri *et al*., 1989), although its mechanism is still unknown.

It is also unclear what the cellular targets of vanillin are, and how vanillin inhibits yeast growth and fermentation (Palmqvist *et al*., 2000). Besides yeast, vanillin has been reported to have several effects on intracellular molecules. It inhibits non-homologous DNA end-joining by inhibiting DNA dependent protein kinase (Durant *et al*., 2003). It also inhibits matrix metalloproteinase-9 expression in human hepatocellular carcinoma cells (Liang *et al*., 2009) and induces apoptosis and cell cycle arrest of human colorectal cancer cells (Ho *et al*., 2009). And more, vanillin is recently

identified from screening of gluconeogenesis inhibitor (Hashimoto *et al*., 2009). This screening was intended for 40,508 samples and vanillin was selected as a lead compound of anti-type II diabetic drug. However, the detailed mechanism of these effects and the intracellular targets of vanillin are not clear. Therefore, in my study, I will investigate cellular targets of vanillin using budding yeast, *Saccharomyces cerevisiae*.

Our laboratory recently developed an image profiling method to identify drug targets based on morphological changes of *Saccharomyces cerevisiae* induced by addition of drugs (Ohnuki *et al*., 2010). The key point is quantification of the morphology of drug-treated yeast phenotype using CalMorph. It was constructed as an image-processing program to extract various morphological data from the digital images representing actin cytoskeleton, cell wall and nucleus microscopic images (Ohtani *et al*., 2004). By analyzing 4718 non-essential gene deleted mutants with this program, we can extract 501 quantitative morphological data (Ohya *et al*., 2005).

The image profiling method to identify drug targets is based on the premise that the morphology of yeast cells treated with the compound are similar with that of mutants which are deleted with the target gene of the compound. According to this idea, the method to infer the drug targets uses following three steps: I) characterization and principal component analysis (PCA) of the 4718 deletion mutants; II) characterization

and PCA of wild-type cells treated with the chemical compound; and III) correlation analysis of the compound-treated wild-type cells and mutants (details in “Materials and Method”).

Ohnuki *et al* have developed the above method and proved that it was applicable to the target-known drugs; Hydroxyurea, concanamycin A and lovastatin (Ohnuki *et al*., 2010). This image profiling method will lead to more detailed knowledge of interactions between vanillin and yeast. Therefore I decided to apply this method to infer vanillin targets and to obtain knowledge of vanillin-action on yeast cells.

Results

Vanillin-target prediction based on morphological changes of wild-type cells

First, I checked growth inhibition effects of vanillin on wild-type cells (Figure 2). It showed a slight delay in growth at 1mM vanillin. Next, I tried to predict targets of vanillin based on morphological changes of wild-type cells. The image profiling method I selected in this study needs morphological data of yeast cells treated with a drug at concentrations which cause a slight delay in the growth rate. Then, wild type cells were treated with 0, 0.25, 0.50, 0.75 and 1.00 mM vanillin and photographed. Each experiment was repeated five times. Images were analyzed using CalMorph (Figure 3) and 501 morphologic parameter values were obtained.

98 of the 501 parameter values were found to show significant dose-dependent changes at false discovery rate (FDR) = 0.20 of Jonckheere-Terpstra test (Table 1). CalMorph parameters “Whole cell size” in all cell cycle stages were detected in the 98 parameters (C11-1A: rank 19, C101_A1B: rank 8, C101_C: rank 64) indicating that the cell size of vanillin-treated wild-type cells was reduced in a dose-dependent manner (Figure 4).

To identify gene-deleted cells with similar morphologic profiles to vanillin-treated wild-type cells, I applied the method as described previously (Ohnuki *et*

al., 2010). Among the morphologic profiles of 4718 non essential-gene disruption mutants, 95 (2%) were significantly similar with that of the vanillin-treated cells at $P < 0.05$ with the Bonferroni correction and maximum value of correlation coefficient (R_{max}) was 0.638 (Figure 5).

To investigate functional relationship among top-ranked gene products, I used gene ontology (GO). Among the 30 top-ranked genes ($R > 0.472$), 5 genes were categorized as belonging to "cytosolic large ribosomal subunit" with the GO database (GO ID: 22625) and significant enrichment of genes annotated to the term was observed 1.4% (109 out of 4707 background non-essential genes) to 16.7% (6 out of 30 top-ranked genes, $P = 0.002$ of binomial test). Table 2 shows GO terms showing significant enrichment categorized among 10-500 top-ranked mutants at $P < 0.01$. These results indicate that vanillin reduced yeast cell size and that it may affect large ribosomal subunit and reduce cell size. However, the inference results may be uncertain, since the relatively low maximum value of correlation coefficient of morphologic profiles ($R_{max} = 0.638$) suggests that morphologic changes of vanillin-treated cells is not so similar to that of candidate mutants.

Vanillin-target prediction based on morphological changes of *erg6*Δ

Recently, genome-wide screening of the genes for tolerance to vanillin was carried out to identify 76 mutants as vanillin-sensitive mutants (Endo *et al*., 2008) and the author indicated ergosterol is involved in tolerance to vanillin, although the mechanism of vanillin tolerance was still arguable (Endo *et al*., 2009). I thought that if the genes involved in ergosterol biosynthesis pathway have any interactions with vanillin, the morphology of the gene-deleted cells treated with vanillin may be different from that of wild-type cell because of its sensitivity to vanillin. So, I applied the image profiling method with *erg6*Δ which is a mutant of ergosterol biosynthesis pathway and has sensitivity to vanillin (Endo *et al*., 2008) to investigate whether the interaction between vanillin and ergosterol exists or not.

Similar to the procedure performed with wild-type cells, I checked growth inhibition effects of vanillin on *erg6*Δ (Figure 6). Consistent with a previous report, *erg6*Δ exhibited vanillin sensitivity and extended lag time. Then, *erg6*Δ cells were treated with 0, 0.25, 0.50, 0.75 and 1.00 mM vanillin, and the images were analyzed by CalMorph (Figure 7).

131 of the 501 parameters were found to show dose-dependent changes at FDR = 0.20 of Jonckheere-Terpstra test (Table 3). Like wild-type cells, CalMorph parameters

"Whole cell size" in all cell cycle stages were detected in the 131 parameters (C11-1A: rank 92, C101_A1B: rank 70, C101_C: rank 93) indicating that the vanillin treatment reduced the cell size of *erg6*Δ in a dose-dependent manner (Figure 8).

Image profiling revealed that among the morphologic profiles of 4718 non essential-gene disruption mutants, 123 (2.6%) were significantly similar with that of the vanillin-treated *erg6*Δ at $P < 0.05$ with the Bonferroni correction and R_{max} was 0.653 (Figure 9).

Among the 30 top-ranked genes ($R > 0.517$), 5 genes were showing significant enrichment categorized as belonging to "cytosolic large ribosomal subunit" with the GO database (GO ID: 22625) and significant enrichment of genes annotated to the term was observed 1.4% (109 out of 4707 background non-essential genes) to 16.7% (6 out of 30 top-ranked genes, $P = 0.002$ of binomial test), that is the same result as wild-type cells. Table 4 shows GO terms categorized among 10-500 top-ranked mutants at $P < 0.01$. Most of the terms detected in this experiment are related to ribosome although "vesicle fusion" and "endoplasmic reticulum membrane" were also detected.

To confirm if the results are similar between wild-type cells and *erg6*Δ or not, I investigated correlation coefficient between the R values of these two strains (Figure 10). Calculated correlation coefficient value was 0.713 at $P < 2.2\times10^{-16}$. This result means morphological features were similar between these two strains. As discussed

above, I think that morphological features may be different if the genes involved in ergosterol biosynthesis pathway have any interactions with vanillin. Thus, the result suggests that ergosterol is not a direct target of vanillin and that loss of ergosterol caused by *ERG6* deletion aggravates vanillin effect on intercellular targets.

Vanillin bio-conversion in yeast

In *Saccharomyces cerevisiae*, it has been reported that vanillin is able to be converted to its respective alcohol and acid derivatives (Fitzgerald *et al*., 2003), and also indicated that vanillin is catalyzed by Adh6p and Adh7p *in vitro* (Larroy *et al*., 2002a, b). In my previous experiment, since vanillin in the medium maybe catalyzed by Adh6p or Adh7p, the results may reflect the effect of reduction of vanillin and/or increase of its catabolite. Therefore it is needed to use the yeast strain that cannot convert vanillin to its metabolite in order to investigate effect of vanillin more accurately.

To check if *adh6*Δ and *adh7*Δ mutants cannot convert vanillin *in vivo*, I first investigated vanillin reduction ratio in YPD medium inoculated with the mutants (Figure 11A). As expected, vanillin concentration was reduced in wild-type culture. Contrary, most of vanillin was remained in YPD medium inoculated with *adh6*Δ after 24 h culture although *adh7*Δ consumed most of it. Thus the results suggest that Adh6p plays more important role of vanillin bio-conversion than Adh7p *in vivo*. This

suggestion is consistent with the report that indicates low expression level of *ADH7* (Petersson *et al*., 2006).

Vanillin-target prediction based on morphological changes of wild type cells deleted *ADH6*

From the result of measurement vanillin concentration in yeast cultures, I produced *his3*Δ *adh6*Δ strain (details in "Materials and Methods") to investigate morphological changes of cells treated with vanillin which dose is graded accurately. First, I measured vanillin concentration inoculated with the produced strain and wild-type cells (*his3*Δ) (Figure 11B, 12) and confirmed *his3*Δ *adh6*Δ shows similar ability of vanillin bio-conversion with *adh6*Δ.

Next, I checked growth inhibition effects of vanillin on *his3*Δ *adh6*Δ (Figure 13). The strain exhibited growth delay at 1 mM vanillin although additional sensitivity was not found compared to wild-type. Then, *his3*Δ *adh6*Δ cells were treated with 0, 0.25, 0.50, 0.75 and 1.00 mM vanillin, and the images were analyzed by CalMorph (Figure 14).

63 of the 501 parameters were found to show dose-dependent change at FDR=0.20 of Jonckheere-Terpstra test (Table 5). CalMorph parameters "Whole cell size"

in stageA (unbudded cells with one nucleus) and stageA1B (budded cell with one nucleus) were detected in the 63 parameters (C11-1A: rank 14, C101_A1B: rank 23) indicating that the cell size of vanillin treated *his3*Δ *adh6*Δ was reduced in a dose-dependent manner (Figure 15).

Image profiling revealed that among the morphologic profiles of 4718 non essential-gene disruption mutants, 252 (5.3%) were significantly similar with that of the vanillin-treated *his3*Δ *adh6*Δ at $P < 0.05$ with the Bonferroni correction and R_{max} was 0.719 (Figure 16). Higher R_{max} of *his3*Δ *adh6*Δ than wild-type suggests that the effect of vanillin was appeared more accurately because of *ADH6* deletion.

Among the 10 top-ranked genes ($R > 0.559$), 3 genes were categorized as belonging to "cytosolic large ribosomal subunit" with the GO database (GO ID: 22625) and significant enrichment of genes annotated to the term was observed 1.4% (109 out of 4707 background non-essential genes) to 30% (3 out of 10 top-ranked genes, $P = 0.00832$ of binomial test), that is the similar result with other two strains. Table 6 shows GO terms showing significant enrichment categorized among 10~500 top-ranked mutants at $P < 0.01$. Most of the terms detected in this experiment were related to ribosome although "regulation of cell size" and "mitochondrion" were also detected.

Similar to the experiment of *erg6*Δ, I investigated correlation coefficient between the R values of wild-type and *his3*Δ *adh6*Δ (Figure 17). Calculated correlation

coefficient value was 0.8340 at $P < 2.2 \times 10^{-16}$, which was higher than that between wiled-type and *erg6*Δ. These results indicate that morphological features were similar between these two strains and that deletion of the *ADH6* gene makes morphologic profiling more accurate.

Discussion

In this study, I searched intercellular targets of vanillin. To obtain clues about the targets, I selected the image profiling method developed in our laboratory (Ohnuki *et al*., 2010) with the three yeast strains. The results of the image profiling of wild-type and *erg6*Δ or *his3*Δ *adh6*Δ were highly correlated indicating that vanillin-effects on these two strains are similar with that on wild-type. This also suggests that deletion of these genes do not alter the effect of vanillin on cells and that these gene products are not a direct target of vanillin, because if there is any interaction between genes and compounds, the morphological features of mutants treated with the compounds are thought to be different from that of wild-type cells.

The *erg6*Δ mutant was reported to be sensitive to vanillin (Endo *et al*., 2008) and the author suggested that ergosterol is involved in tolerance to vanillin (Endo *et al*., 2009). However, from the results of image profiling of *erg6*Δ cells, it seems that Erg6p is not a direct target of vanillin as discussed above. Together with the previous report that *erg6*Δ showed sensitivity to other compounds (Markovich *et al*., 2004; Fei *et al*., 2008), *ERG6* deletion aggravates vanillin effects on intercellular targets possibly by incorporation of the compound. The number of predicted genes as candidates of vanillin-targets and the maximum value of calculated correlation coefficient were

increased compared with the result of wild-type (Table 7). This result also supports the idea that amount of incorporated vanillin is increased in the *erg6*Δ cells and vanillin is more effective on the targets than in wild-type.

Adh6p may catalyze vanillin bio-conversion in yeast (Fitzgerald *et al*., 2003; Larroy *et al*., 2002). Consistent with this, vanillin concentration in medium is decreased in wild-type whereas remained in *adh6*Δ mutant (Figure 11) suggesting that vanillin can be converted to its metabolite when Adh6p exists in cells. In the results of *his3*Δ *adh6*Δ, the number of predicted genes as vanillin-targets, the maximum value of calculated correlation coefficient and the enrichment ratio of genes annotated as "ribosomal large subunit" were increased compared with the results of wild-type (Table 7). These results indicate that the accuracy of the image profiling was increased in *his3*Δ *adh6*Δ probably due to the inability of vanillin bio-conversion. It suggests that this condition in *his3*Δ *adh6*Δ makes the effects of vanillin on intercellular targets more aggravate.

It is still questionable that why *his3*Δ *adh6*Δ did not show severer vanillin sensitivity than wild-type although vanillin concentration remained high in *his3*Δ *adh6*Δ medium and profiling results suggested more specific of vanillin effects. One hypothesis is that the growth inhibition effects of vanillin and that of vanillin-metabolite are similar. However, this is unlikely because previous study reported that vanillyl alcohol is a main metabolite of vanillin in *Saccharomyces cerevisiae* and its growth inhibition effects on

yeast cells are very weak compared with vanillin (De Wulf and Thonart, 1989; Fitzgerald *et al*., 2003). So, other reasons are still considerable how vanillin delays yeast growth.

Previous studies reported that the phenolic compounds inhibit enzyme activities (Rico-Munoz *et al*., 1987; Wendakoon and Sakaguchi, 1995) and that yeast cannot bio-convert vanillin when its concentration is 15 mM suggesting that vanillin could affect essential metabolic process by directly or indirectly inhibiting the oxidoreductase (Fitzgerald *et al*., 2003). However, the result of the morphological features of *his3*Δ *adh6*Δ suggests that vanillin does not affect its metabolic pathway because if vanillin affects its metabolic pathway, *his3*Δ *adh6*Δ might exhibit different morphology from wild-type.

In common among wild-type, *erg6*Δ and *his3*Δ *adh6*Δ, the genes annotated as "ribosomal large subunit" were significantly enriched in the top of predicted target genes. For example, wild-type cells treated with vanillin showed similar morphology with *rpl19a*Δ cells (the correlation coefficient was 0.638 and the P value with the Bonferroni correction was 1.5×10^{-9}). I think this enrichment is vanillin specific because it becomes high in *his3*Δ *adh6*Δ mutants which can exhibit more accurate effect of vanillin.

Only in the profiling results of *his3*Δ *adh6*Δ, another gene-enrichment was

significantly detected in the term “mitochondrion” (P = 0.001). It might be consistent with the previous study that vanillin tolerant yeast strain up-regulated the genes involved in complex III of the mitochondrial respiratory chain (Endo *et al*., 2009).

Also, I revealed that vanillin reduced cell size of the three yeast strains. Generally, the mutants of the genes related to ribosome show small cell size in normal conditions. For example, *rpl19a*Δ which is a mutant of large ribosomal subunit decreases its cell size (Jorgensen *et al*., 2002). Therefore, reduced cell size is a common feature of vanillin-treated cells and mutants of ribosome large subunits.

The loss of ribosomal function is seemed to be the reason of reduced cell size in vanillin treatment as discussed above. Moreover, a previous report also suggests that the loss of ribosomal function seems to cause sensitivity to vanillin. The report shows that the six mutants of ribosomal protein (*rpl21a*Δ, *rpl6b*Δ, *rps21a*Δ, *rpl37a*Δ, *rpl12b*Δ and *mrps35*Δ) were contained in the 76 vanillin-sensitive mutants (Endo *et al*., 2008). Together with my results and the previous report suggest that vanillin might affect yeast ribosome itself or related function, leading reduced yeast cell size.

Materials and Methods

Yeast strains and growth conditions

Strains used in this study are shown in Table 8. Cells were grown in YPD medium contained 1% Bacto-yeast extract (Becton, Dickinson and Company, USA), 2% polypeptone (Becton, Dickinson and Company) and 2% glucose (Nacalaitesque, Japan) with or without vanillin at 25°C. amples for analyses by CalMorph were taken in the log-phase of growth (4×10^{6} ~ 1×10^{7} cells/ml). In selection of transformed cells, it were grown in synthetic growth (SD) medium contained 0.67% yeast nitrogen base without amino acids (Becton, Dickinson and Company), 2% glucose, and 20 mg/ml supplements (adenine sulfate, uracil, L-tryptophan, L-histidine-HCl, L-lysine-HCl and L- methionine).

Chemicals

Stock solutions of 2 M vanillin (Kanto Chemicals, Japan) were prepared in DMSO (Wako Chemicals, Japan) and stored at -20 °C.

Growth inhibition effects of vanillin

Cells were pre-cultured and inoculated in 96-well plate with various

concentration of vanillin. Starting concentration was 3×10^4 cells/ml and OD_{600} was measured with SPECTRAmax (Molecular Devices, USA) at 0 time and each 1.5 hour after over-night culture (about 14-16 hours). Doubling time was calculated with the most inclined four data point of the growth curve and relative growth inhibition ratio was calculated from the data.

Fluorescence staining and microscopy

Logarithmically growing cells were fixed for 30 min in the growth medium supplemented with formaldehyde (final concentration; 3.7%) and potassium phosphate buffer (100 mM, pH 6.5) at 25°C. Cells were sedimented by centrifugation and were further incubated in potassium phosphate buffer containing 4% formaldehyde for 45 min at room temperature. Actin staining was performed by overnight treatment with 15 U/ml Rhodamine-phalloidin (Molecular Probes, Inc., Eugene, OR, USA) in PBS with 1% Triton-X. Then, the cells were mixed with 1 mg/ml FITC-ConA (Sigma, St. Louis, MO, USA) in P buffer (10 mM sodium phosphate, and 150 mM NaCl, pH 7.2) for 10 min to stain mannoprotein on the cell surface. After washing with P buffer twice, the cells were mixed with mounting buffer (1 mg/ml p-phenylenediamine, 25 mM NaOH, 10% PBS and 90% grycerol) containing 20 μg/ml 4’-6’-diamidino-2-phenylindole

(DAPI, Sigma) for DNA staining. Specimens were observed with Axioimager with a ×100 ECplan-Neofluar lens (Carl Zeiss, Germany) equipped with CoolSNAP HQ cooled-CCD camera (Roper Scientific Photometrics, Tucson, AZ, USA) and Axio Vision software (Carl Zeiss).

Image processing and statistical analysis

Image-processing analysis was performed with CalMorph (ver.1.2). CalMorph is a program that can obtain a large amount of data as many morphological parameters automatically on cell cycle phase, cell forms, etc., for individual cells, from a set of pictures of cell walls, cell nuclei, and actins. CalMorph user manual is available at SCMD (Saito *et al*., 2004; http://scmd.gi.k.u-tokyo.ac.jp/datamine/).

Statistical analysis was performed with the Java program as described previously (Ohnuki *et al*., 2010). The Java program executes the Jonckheere-Terpstra test, PCA , Pearson product-moment correlation analysis and bootstrap-based estimation of the False Discovery Rate (FDR).

To calculate principal component (PC) scores of wild-type cells treated with the chemical compound, the 501 morphological parameters were summarized into Z score from Jonckheere-Terpstra test. Each Z score represents the dose-dependency of

the parameter under a normal distribution. Then, the 104 PC scores were obtained and these scores represent the altered morphologic profile that resulted from treatment with the compound.

To evaluate similarities between morphologic changes in drug-treated wild-type cells and mutant strains, correlation coefficient R and the associated P value for the 104 principal component scores from wile-type cells treated with the compound and mutants are calculated.

Gene ontology terms

The information of gene ontology annotations used in this study was "GO Term Finder" (http://www.yeastgenome.org/cgi-bin/GO/goTermFinder.pl) in the Saccharomyces Genome Database (SGD) website. Query genes were obtained from the analyzed CalMorph data and background-gene set was 4707 genes of 4718 non-essential genes, associated with at least one GO term.

ADH6 gene deletion

The procedures of *ADH6* deletion are shown in Figure 18. PCR was performed using Ex Tax Kit (TaKaRa, Kyoto, Japan) Plasmid used in this study was pYO2241 (pBS-*Cg LEU2*).A set of primers (Forward 5'-CATTCGAGGAA GAAATTCAACACAACAACAAGAAAAGCCAAAATCTCGAGGTCGACGGTAT C-3', and Reverse 5'-AGCAGTTAAAAAGAAAGGAGCTACATTTATCAAGAG CTTGACAACCGCTCTAGAACTAGTGGATC-3') was used to amplify *CgLEU2* sequence with up and down 45 base pair of *ADH6* sequence. Amplified PCR products was purified with precipitation and introduced into yeast wild-type cells (*his3*Δ) (Ito *et al*., 1983). Transformants were selected SD medium lacking leucine. Deletion of the ADH6 gene were confirmed by PCR using a set of primers (Forward 5'-CAATTCAATCTAATTTAATA-3', Reverse 5'-TATATCGAT TAAAACAGCAC-3').

Measurement of vanillin concentration in yeast culture

YPD medium containing vanillin were inoculated with yeast cells. At each time during culture, 100 μl samples were removed, centrifuged (12,000rpm for 3min) and the supernatants collected. After 50 times dilution in 100 mM TRIS buffer (pH 7.8), the

vanillin levels were measured spectrophotometrically at 340 nm. The concentration in the supernatants was calculated using the molar extinction coefficient of vanillin established experimentally. (This method is referred to Fitzgerald *et al*., 2003)

Figures

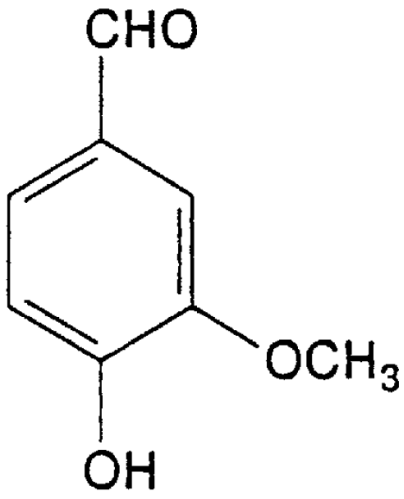

Vanillin

Figure 1. The structure of vanillin (4-hydroxy-3-methoxybenzaldehyde).
(Referred to Walton *et al*., 2003)

A

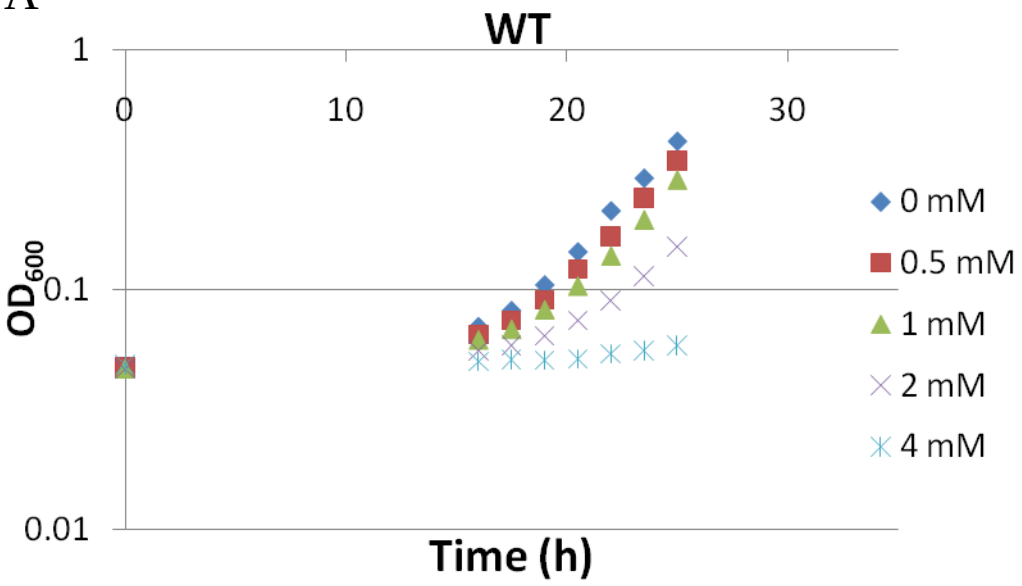

B

Concentration	Doubling Time (h)	Ratio (%)
0 mM	2.72	100
0.5 mM	2.75	101
1 mM	2.81	103
2 mM	3.68	135
4 mM	18.4	677

Figure 2. Growth inhibition effect of vanillin on wild-type cells (*his3*Δ). (A) Wild-type cells (*his3*Δ) were grown in YPD medium contained with indicated concentrations of vanillin at 25 ^{0}C in 96 well plates. OD_{600} was measured by SPECTRA max. Starting concentration was 3×10^{4} cells/ml. "0 mM" contained 0.2% DMSO in YPD. (B) Doubling time was calculated from four data points and normalized to the value at 0 mM to obtain relative inhibition ratio.

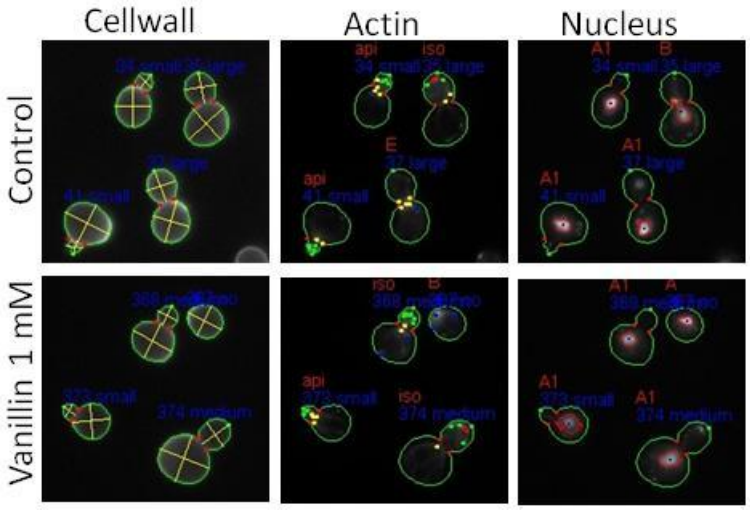

Figure 3. Quantified images of wild-type cells (*his3*Δ) treated with vanillin. Wild-type cells were grown in YPD medium with 1 mM vanillin or 0.1% DMSO (Control) and fixed at the log phase. Cell wall, actin, and nuclei were stained with FITC-ConA, rhodamine-phalloidin and DAPI. Images were quantified by CalMorph. Five experiments for each condition were done and representative images were shown.

A

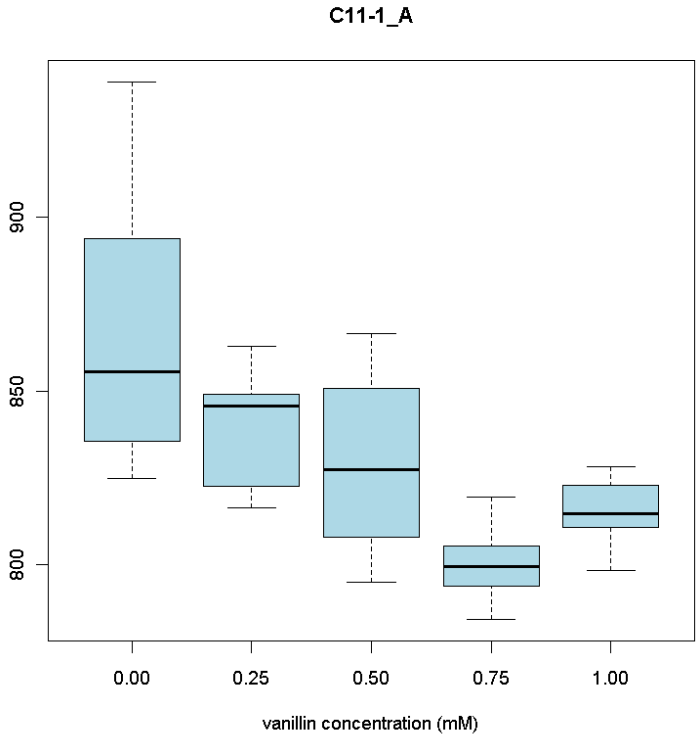
C11-1_A
900
850
800
0.00
0.25
0.50
0.75
1.00
vanillin concentration (mM)

B

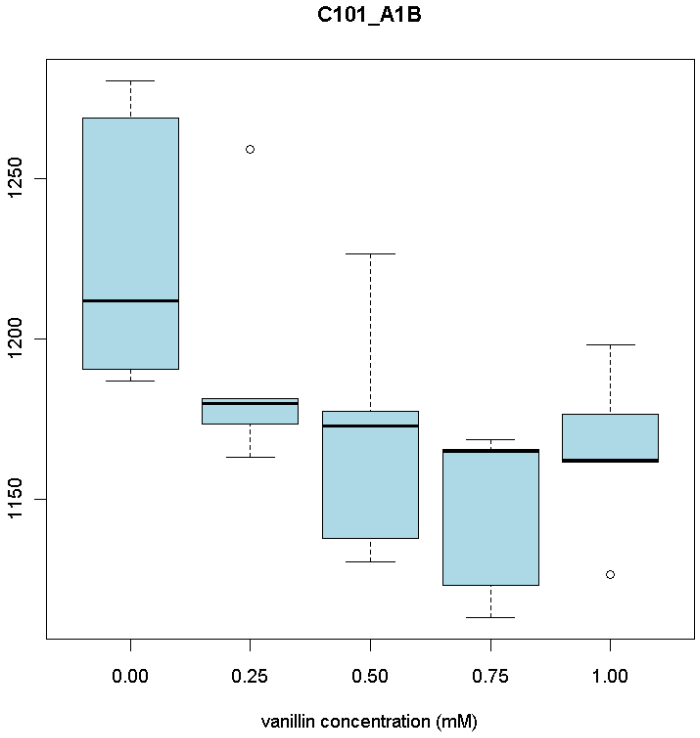
C101_A1B
1250
1200
1150
0.00
0.25
0.50
0.75
1.00
vanillin concentration (mM)

C

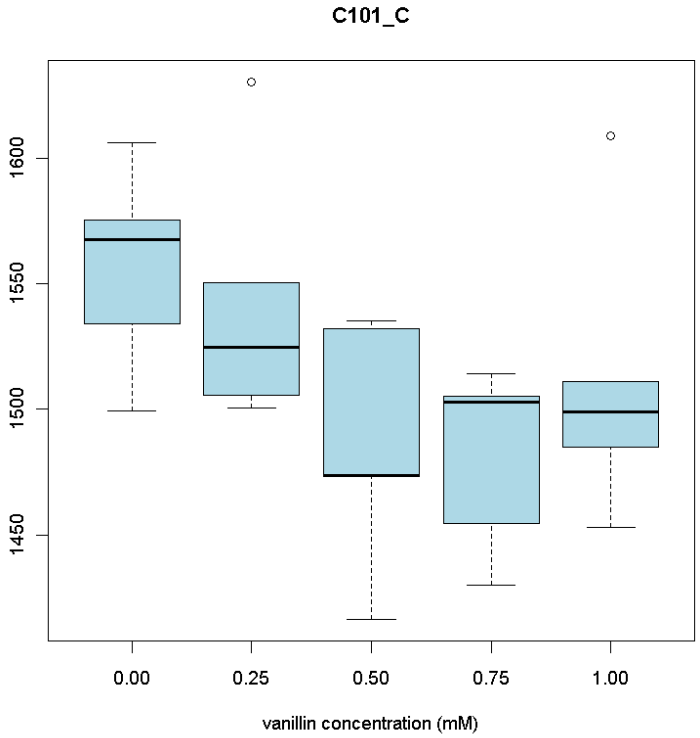

D

Parameter	Z value	P value	Q value
C11-1_A	-2.892	0.004	0.063
C101_A1B	-3.227	0.001	0.037
C101_C	-2.223	0.026	0.131

Figure 4. Box plot of whole cell size of wild-type cells (*his3*Δ) treated with vanillin. Wild-type cells were grown in YPD medium with inhibited concentrations of vanillin, photographed and analyzed by CalMorph. Experiments were repeated five times for each vanillin concentration. (A) CalMorph parameter "C11-1_A" indicates whole cell size of unbudded cells with one nucleus. (B) CalMorph parameter "C101_A1B" indicates whole cell size of budded cell with one nucleus. (C) CalMorph parameter "C101_C" indicates whole cell size of budded cell with two nuclei. (D) Results of Jonckheere-Terpstra test of these parameter values. Z value indicates how degree cells change its morphology with vanillin dose-dependent manner, plus means increase and minus means decrease.

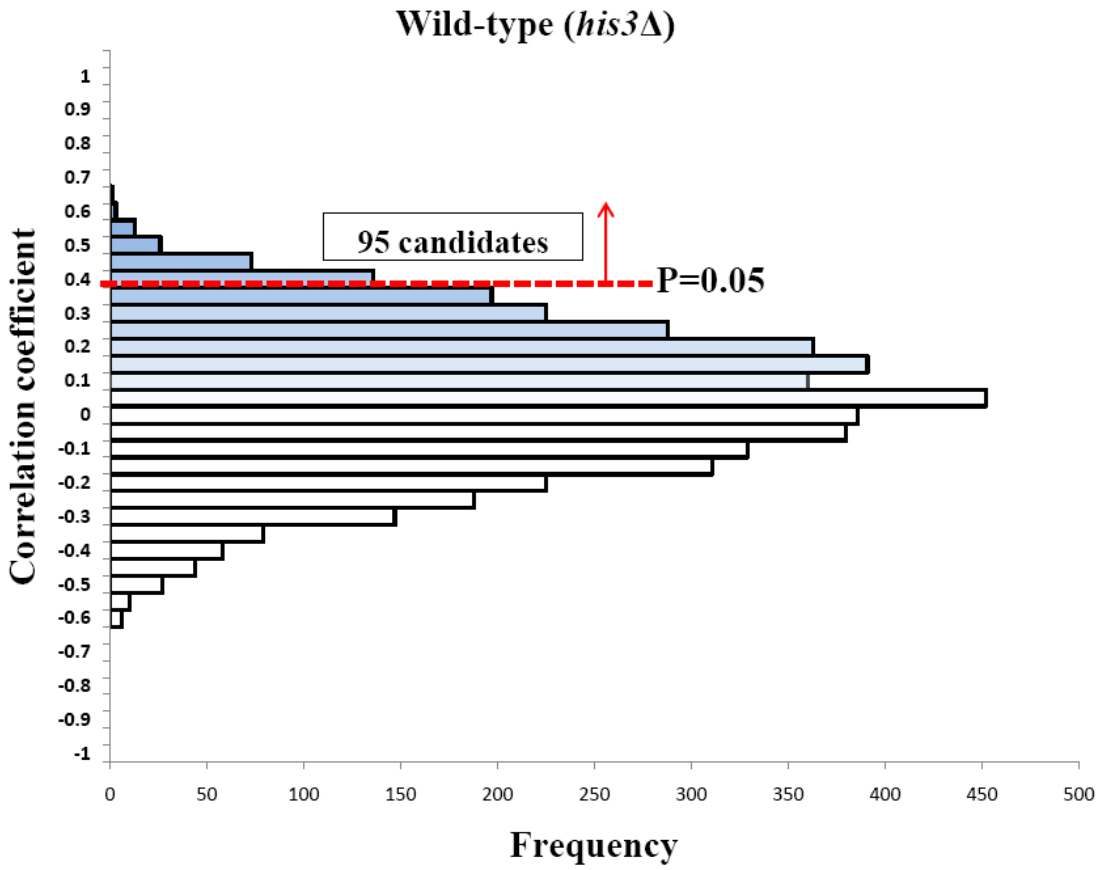

Figure 5. Histogram of correlation coefficient of morphological profiles between 4718 mutants and wild-type cells (*his3*Δ) treated with vanillin. Morphological data of wild-type cells treated with vanillin was analyzed by the Java program (Ohnuki *et al*., 2010). Vanillin concentrations were 0.00, 0.25, 0.50, 0.75, 1.00 mM and each experiment was repeated five times. The number of candidates detected at P value < 0.05 with the Bonferroni correction was 95. Maximum value of correlation coefficient was 0.638.

A

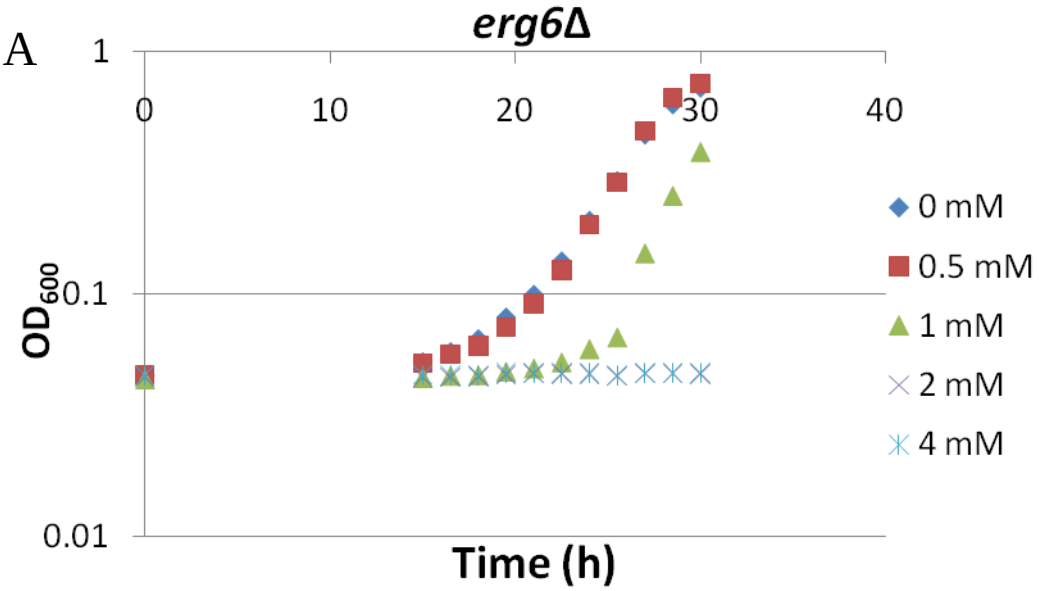

B

Concentration	Doubling Time (h)	Ratio (%)
0 mM	2.62	100
0.5 mM	2.37	91
1 mM	3.23	124
2 mM	78.3	2991
4 mM	124	4744

Figure 6. Growth inhibition effect of vanillin on *erg6*Δ. (A) *erg6*Δ were grown in YPD medium contained with indicated concentrations of vanillin at 25 ^{0}C in 96 well plates. OD_{600} was measured by SPECTRA max. Starting concentration was 3×10^{4} cells/ml. "0 mM" contained 0.2% DMSO in YPD. (B) Doubling time was calculated from four data points and normalized to the value at 0 mM to obtain relative inhibition ratio.

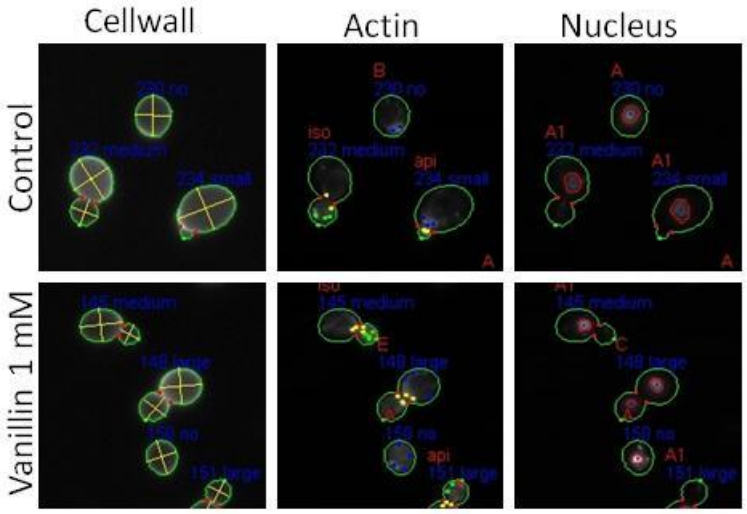

Figure 7. Quantified images of *erg6*Δtreated with vanillin. *erg6*Δ were grown in YPD medium with 1 mM vanillin or 0.1% DMSO (Control) and fixed at the log phase. Cell wall, actin, and nuclei were stained with FITC-ConA, rhodamine-phalloidin and DAPI. Images were quantified by CalMorph. Five experiments for each condition were done and representative images were shown.

A

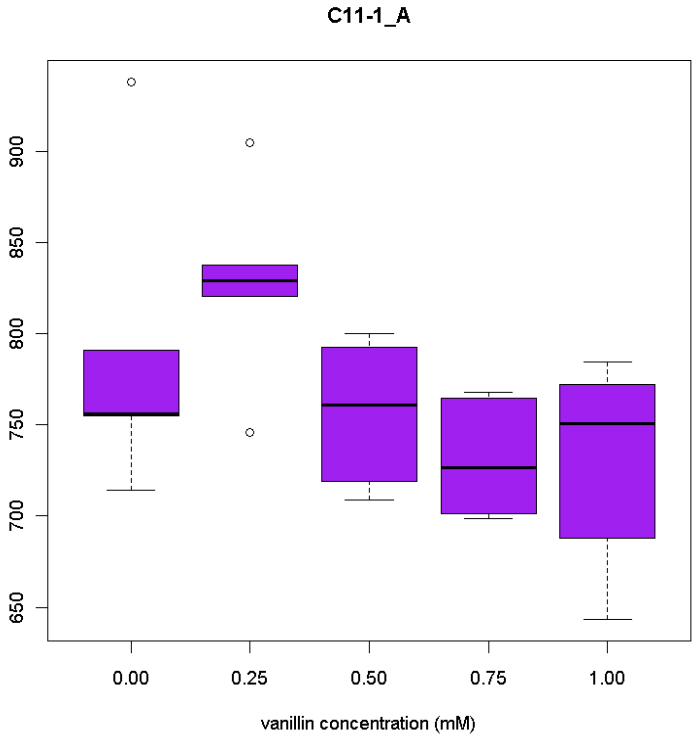
C11-1_A
650
700
750
800
850
900
0.00
0.25
0.50
0.75
1.00
vanillin concentration (mM)

B

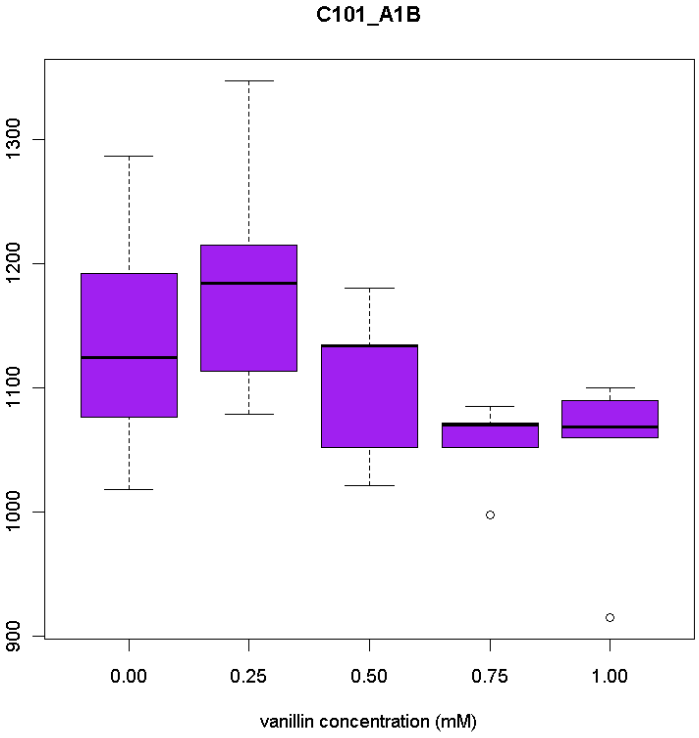
C101_A1B
900
1000
1100
1200
1300
0.00
0.25
0.50
0.75
1.00
vanillin concentration (mM)

C

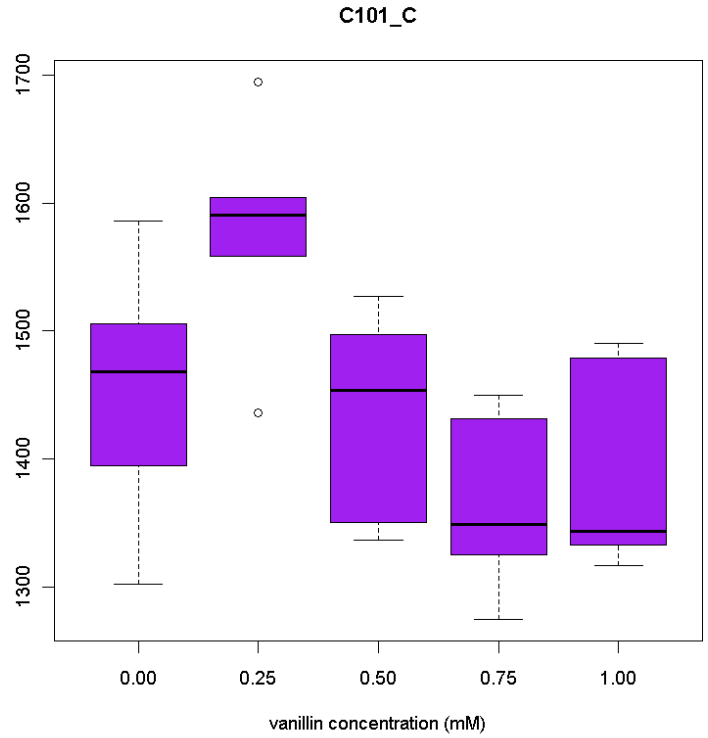

D

Parameter	Z value	P value	Q value
C11-1_A	-2.701	0.007	0.042
C101_A1B	-2.319	0.020	0.077
C101_C	-2.128	0.033	0.097

Figure 8. Box plot of whole cell size of *erg6*Δ treated with vanillin. *erg6*Δ were grown in YPD medium with inhibited concentrations of vanillin, photographed and analyzed by CalMorph. Experiments were repeated five times for each vanillin concentration. (A) CalMorph parameter "C11-1_A" indicates whole cell size of unbudded cells with one nucleus. (B) CalMorph parameter "C101_A1B" indicates whole cell size of budded cell with one nucleus. (C) CalMorph parameter "C101_C" indicates whole cell size of budded cell with two nuclei. (D) Results of Jonckheere-Terpstra test of these parameter values. Z value indicates how degree cells change its morphology with vanillin dose-dependent manner, plus means increase and minus means decrease.

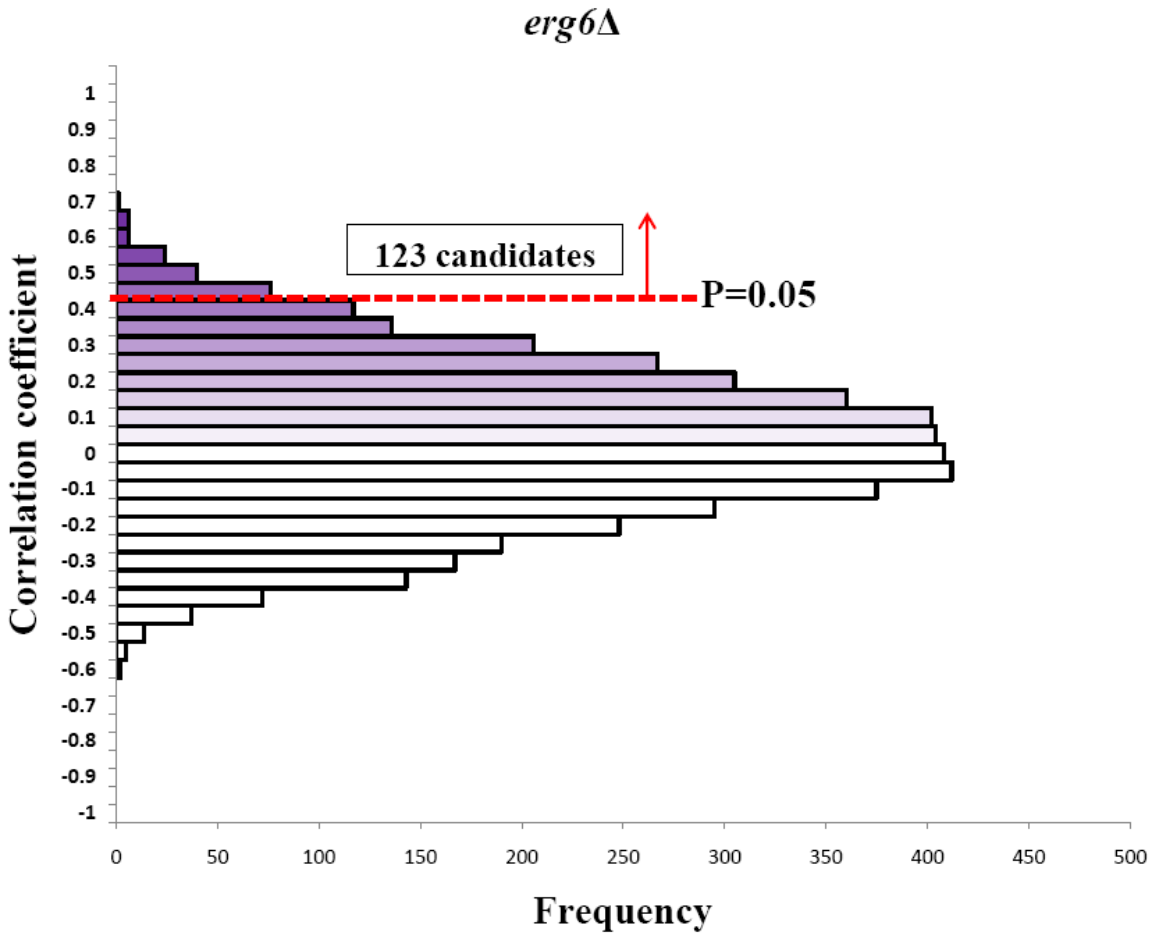

Figure 9. Histogram of correlation coefficient between 4718 mutants and *erg6*Δ treated with vanillin. Morphological data of *erg6*Δ cells treated with vanillin was analyzed by the Java program (Ohnuki *et al*., 2010). Vanillin concentrations were 0.00, 0.25, 0.50, 0.75, 1.00 mM and each experiment was repeated five times. The number of candidates detected at P value < 0.05 with the Bonferroni correction was 123. Maximum value of correlation coefficient was 0.653.

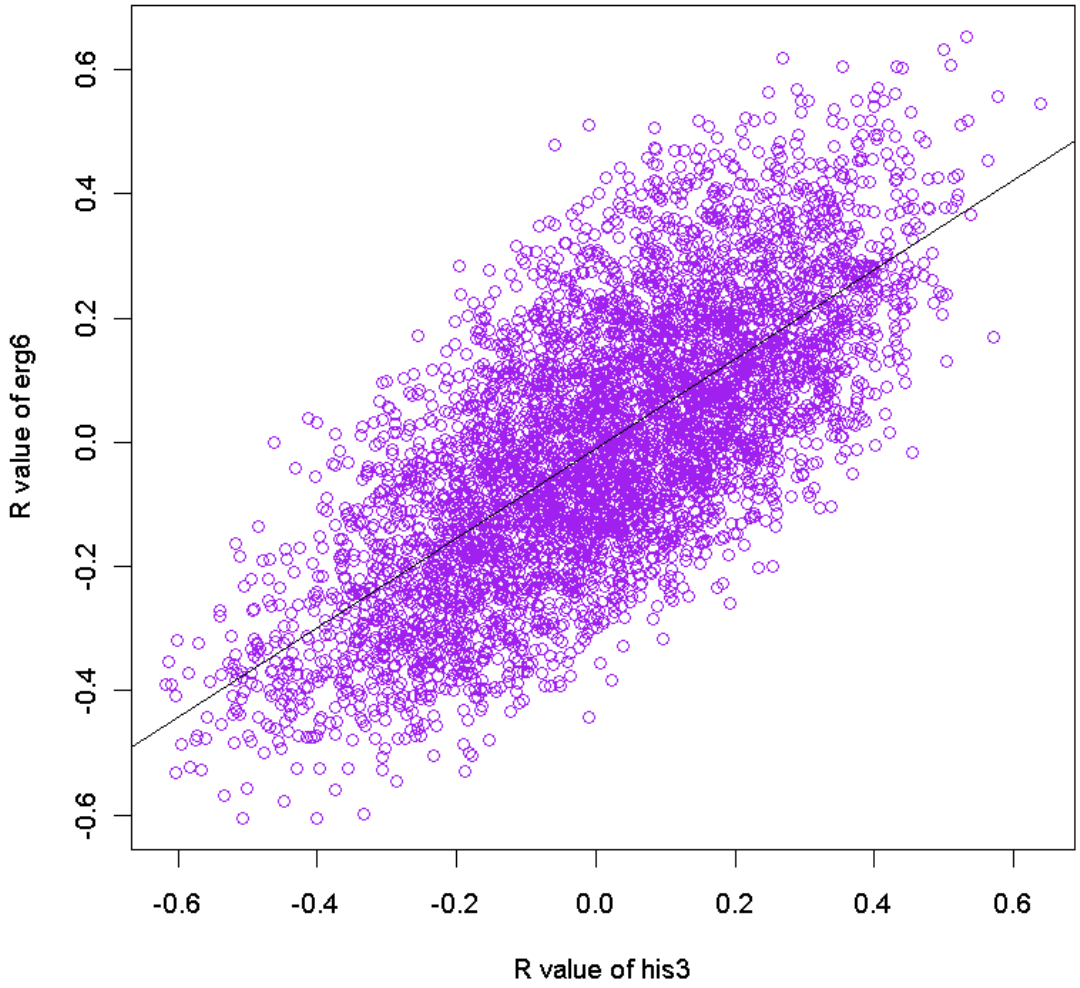

Figure 10. Two-dimensional plot of vanillin treated wild-type (*his3*Δ) and *erg6*Δ. 4718 correlation coefficients (R values) calculated by the image profiling of the two strains (Figure 4 and 8) are plotted. The black line represents a linear regression model ($R = 0.713$ at $P < 2.2\times10^{-16}$).

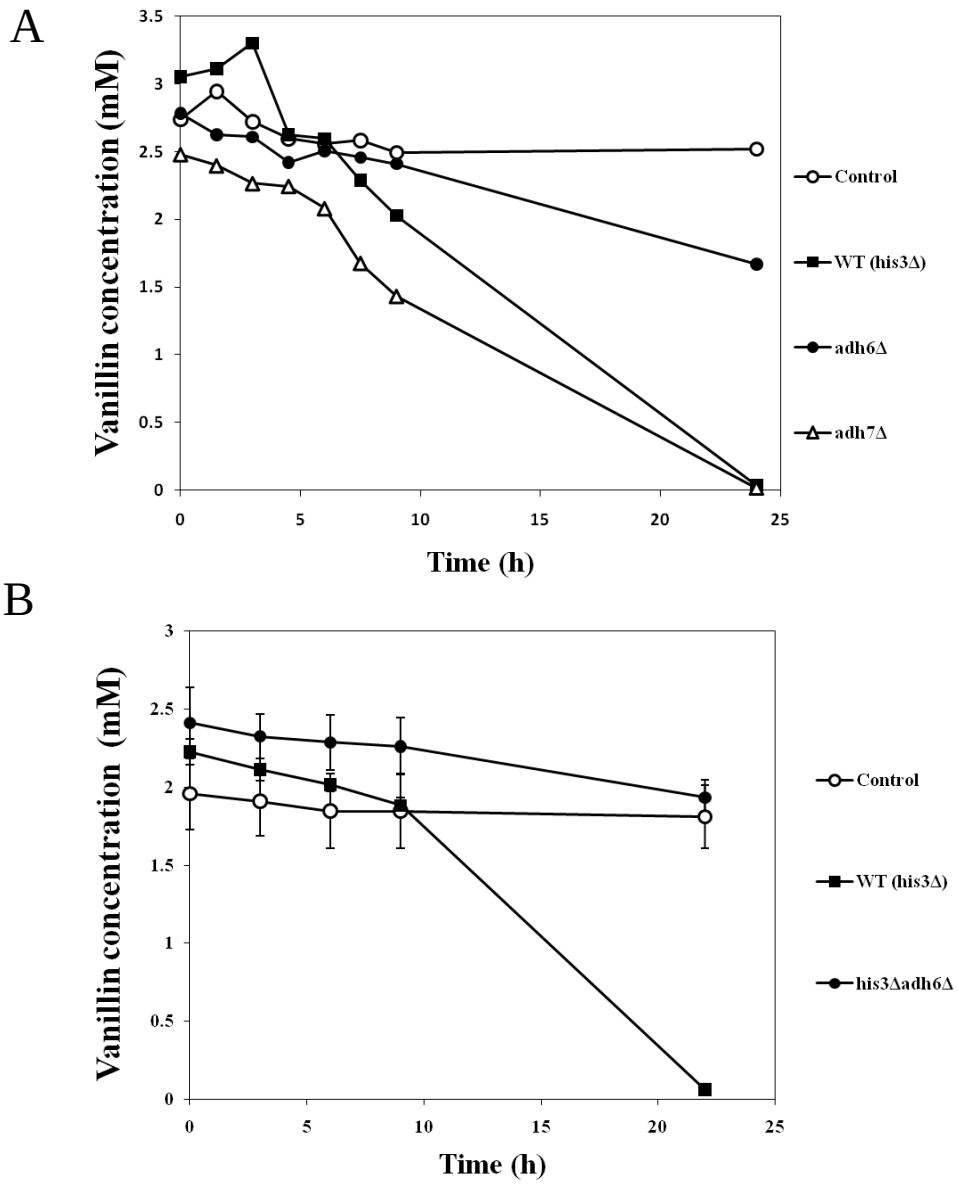

Figure 11. Vanillin concentration in YPD medium inoculated with several yeast strains. (A) Wiled-type (*his3*Δ), *adh6*Δ, and *adh7*Δ were pre-cultured in normal YPD and inoculated at the concentration of 2×10^6 cells/ml in YPD containing 2.5 mM vanillin. "Control" indicates YPD without cells. Supernatants were collected at the indicated time and vanillin concentrations were measured. Experiments were repeated three times. SD calculated from vanillin concentration at each time was shown as bars. (B) Yeast strains, *his3*Δ, and *his3*Δ *adh6*Δ were pre-cultured in normal YPD and inoculated at the concentration of 1×10^7 cells/ml in YPD containing 2 mM vanillin. Other conditions are same as (A).

A

Strain	Reduction ratio (%)	mean	SD
Control (without cells)	9.34 6.91 6.08	7.44	1.70
his3Δ	97.1 97.1 97.2	97.1	0.0707
his3Δ adh6Δ	23.3 16.7 18.9	19.6	3.38

B

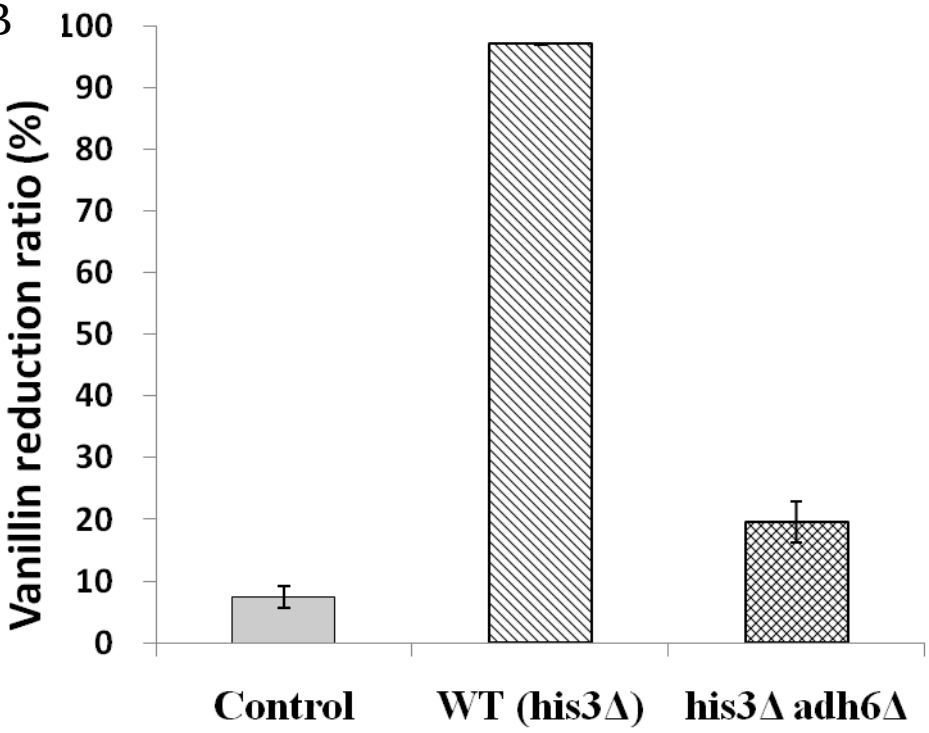

Figure 12. Reduction ratio of vanillin in YPD inoculated with wild-type cells (*his3*Δ) and *his3*Δ *adh6*Δ. (A) Vanillin reduction ratio was calculated from the data of Figure 9 (0h to 22h). (B) Bar graph of vanillin reduction ratio. Each column indicates mean and bar indicates SD.

A

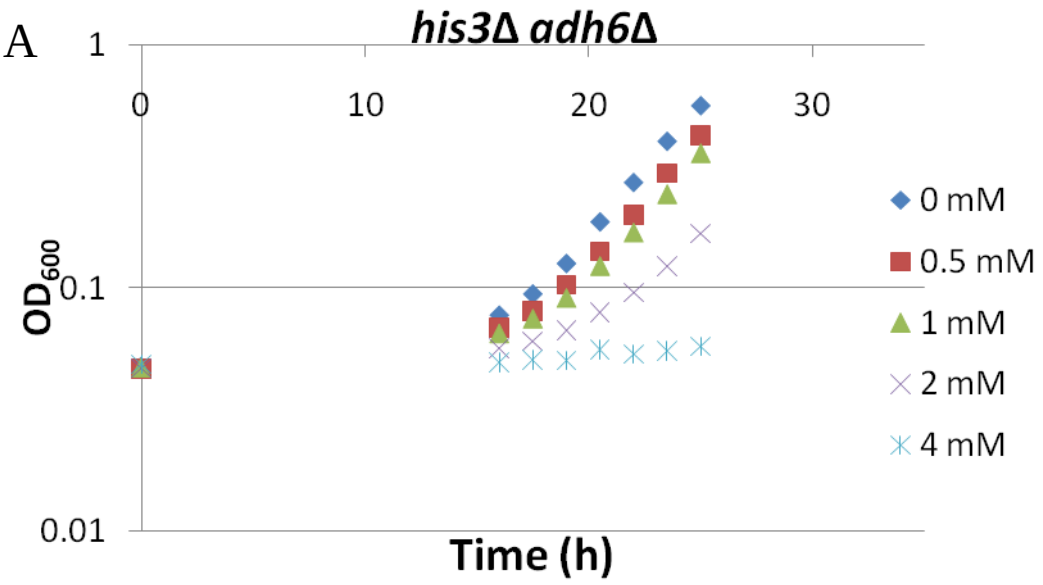

B

Concentration	Doubling Time (h)	Ratio (%)
0 mM	2.55	100
0.5 mM	2.62	103
1 mM	2.71	106
2 mM	3.66	143
4 mM	20.2	790

Figure 13. Growth inhibition effect of vanillin on *his3*Δ *adh6*Δ. (A) *his3*Δ *adh6*Δ were grown in YPD medium contained with indicated concentrations of vanillin at 25 ^{0}C in 96 well plates. OD_{600} was measured by SPECTRA max. Starting concentration was 3×10^{4} cells / ml. "0 mM" contained 0.2% DMSO in YPD. (B) Doubling time was calculated from four data points and normalized to the value at 0 mM to obtain relative inhibition ratio.

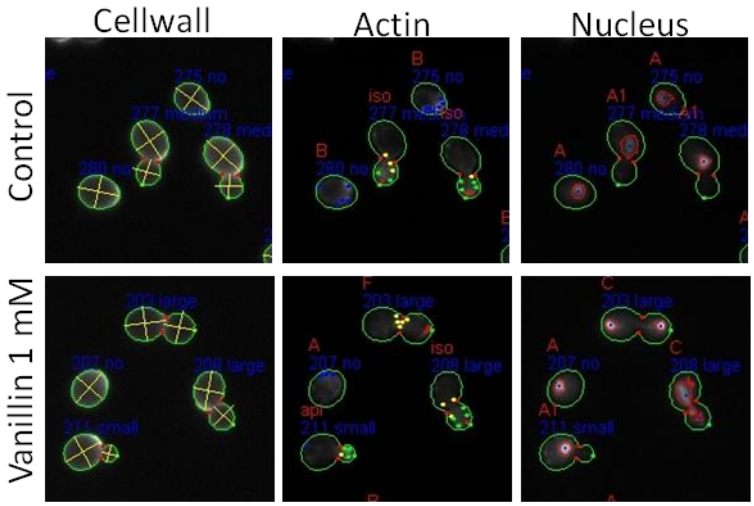

Figure 14. Quantified images of *his3*Δ *adh6*Δtreated with vanillin. *his3*Δ *adh6*Δ were grown in YPD medium with 1 mM vanillin or 0.1% DMSO (Control) and fixed at the log phase. Cell wall, actin, and nuclei were stained with FITC-ConA, rhodamine-phalloidin and DAPI. Images were quantified by CalMorph. Four experiments for each condition were done and representative images were shown.

A

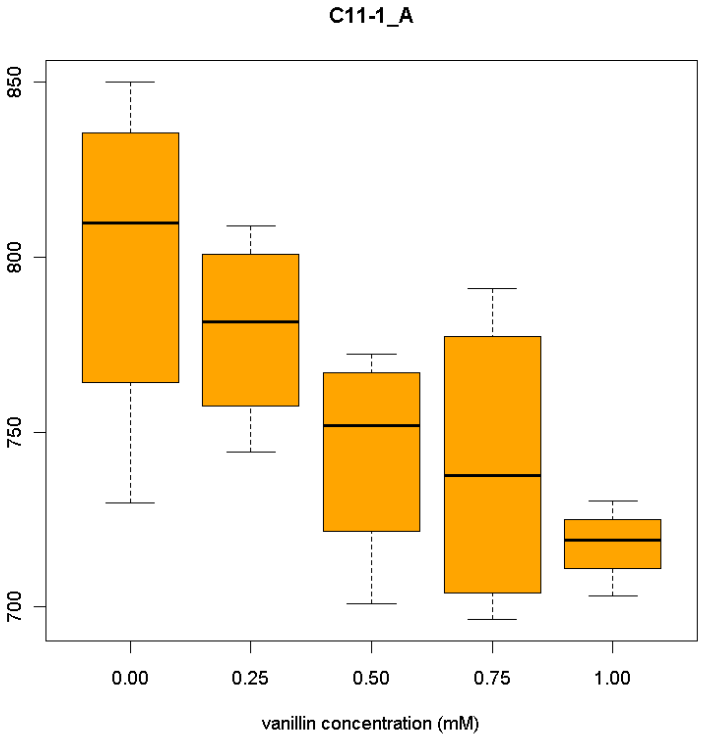
C11-1_A
850
800
750
700
0.00
0.25
0.50
0.75
1.00
vanillin concentration (mM)

B

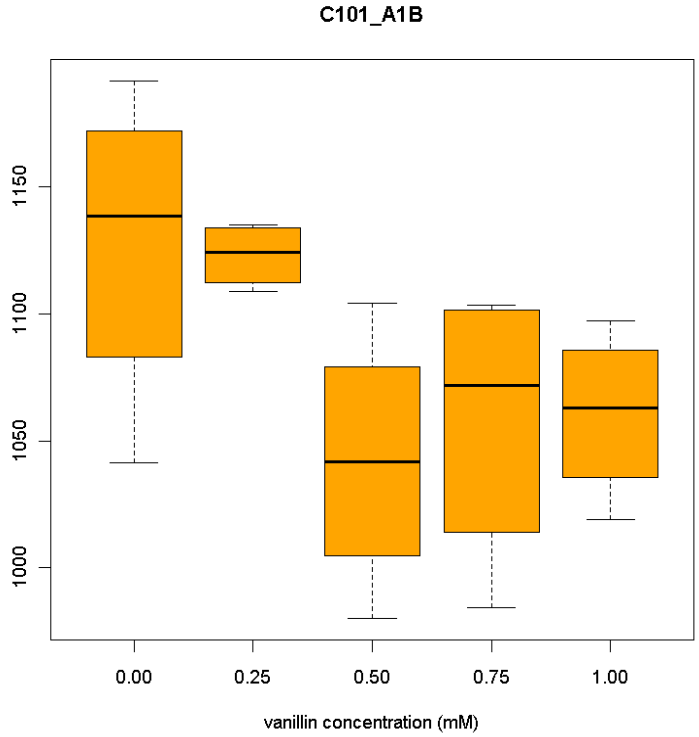
C101_A1B
1150
1100
1050
1000
0.00
0.25
0.50
0.75
1.00
vanillin concentration (mM)

C

Parameter	Z value	P value	Q value
C11-1_A	-2.557	0.011	0.124
C101_A1B	-2.690	0.007	0.106

Figure 15. Box plot of whole cell size of *his3*Δ *adh6*Δ treated with vanillin. *his3*Δ *adh6*Δ were grown in YPD medium with inhibited concentrations of vanillin, photographed and analyzed by CalMorph. Experiments were repeated four times for each vanillin concentration. (A) CalMorph parameter "C11-1_A" indicates whole cell size of unbudded cells with one nucleus. (B) CalMorph parameter "C101_A1B" indicates whole cell size of budded cell with one nucleus. (C) Results of Jonckheere-Terpstra test of these parameter values. Z value indicates how degree cells change its morphology with vanillin dose-dependent manner, plus means increase and minus means decrease.

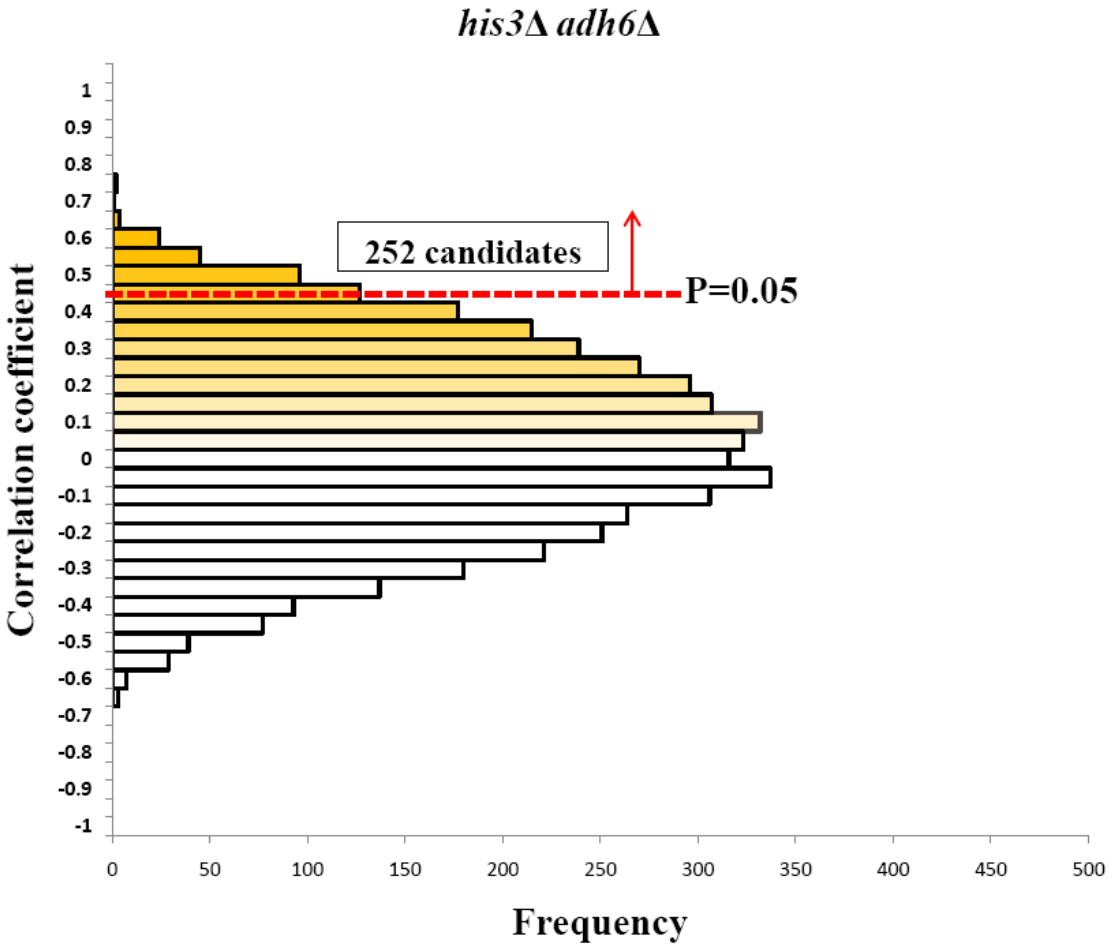

Figure 16. Histogram of correlation coefficient between 4718 mutants and *his3*Δ *adh6*Δ treated with vanillin. Morphological data of *his3*Δ *adh6*Δ cells treated with vanillin was analyzed by the Java program (Ohnuki *et al.*, 2010). Vanillin concentrations were 0.00, 0.25, 0.50, 0.75, 1.00 mg/ml and each experiment was repeated four times. The number of candidates detected at P value < 0.05 with the Bonferroni correction was 252. Maximum value of correlation coefficient was 0.719.

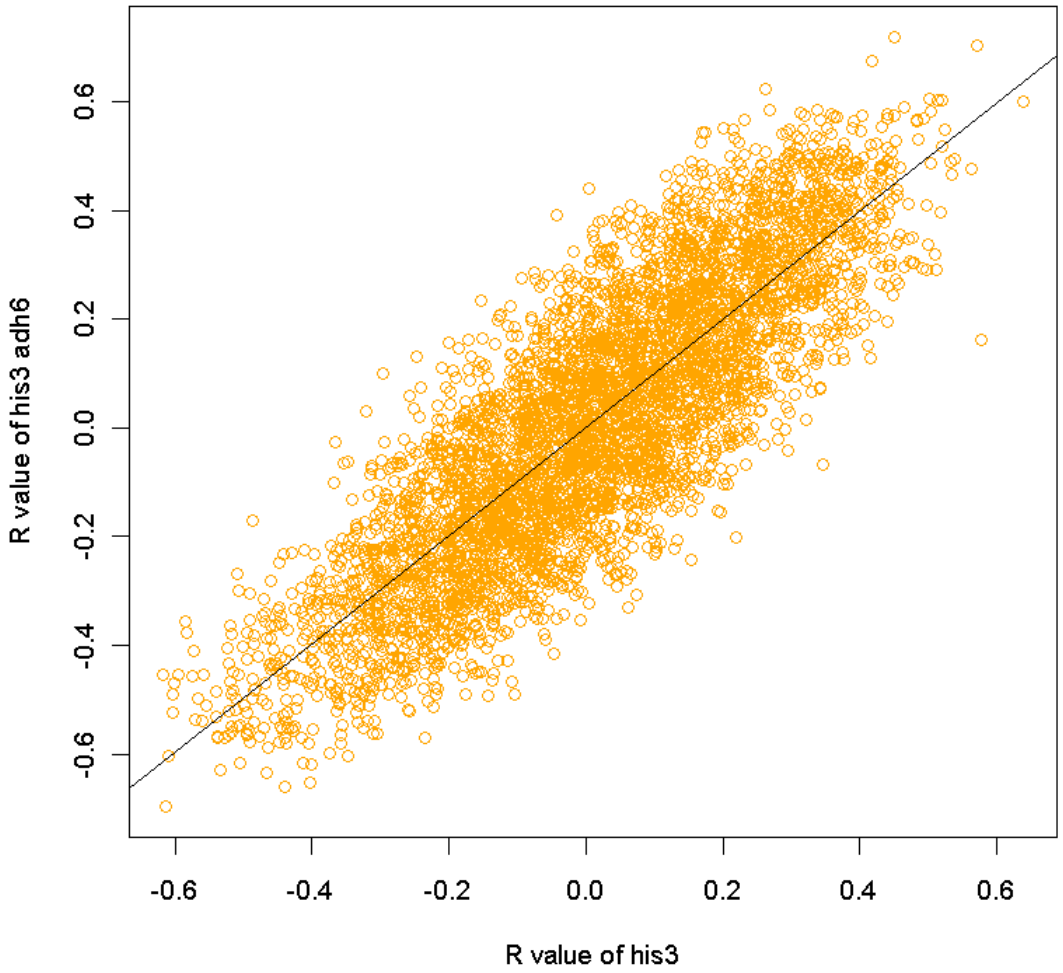

Figure 17. Two-dimensional plot of vanillin treated wild-type (*his3*Δ) and *his3*Δ *erg6*Δ.
4718 correlation coefficients (R values) calculated from the image profiling of the two strains (Figure 4 and 15) are plotted. The black line represents a linear regression model ($R = 0.840$ at $P < 2.2\times10^{-16}$).

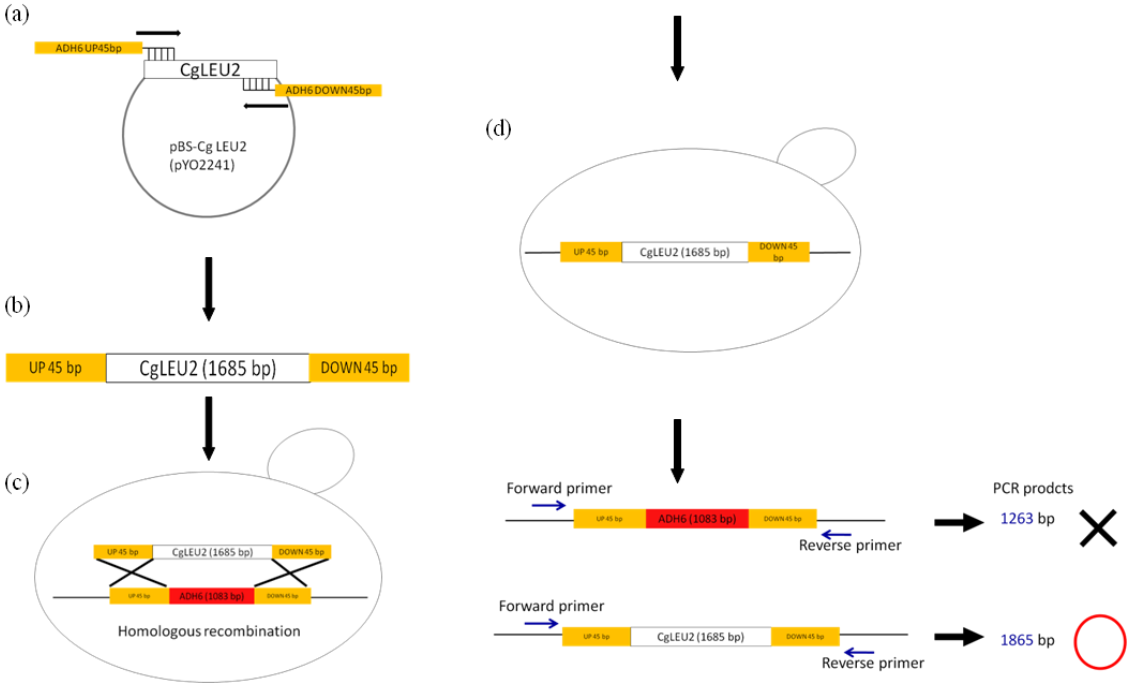

Figure 18. The procedure of *ADH6* disruption. (a)Amplify of *Candida glabrata LEU2* gene (white column) by PCR with a set of primer that have 45 upstream and 45 downstream of *ADH6* complementary sequence (yellow column). (b) DNA fragment derived from (a). (c) Transformation of wild-type strain. In yeast cells, the introduced fragment and *ADH6* gene (red column) are replaced by homologous recombination. (d) Confirmation of transformation. Transformants were selected by the medium without leucine and its genomic DNA was recovered from single colonies. Specific sequence involved in *ADH6* sequence (from *ADH6* 90 upstream and 90 downstream) were amplified by PCR. Finally, *ADH6* genes were deleted if the PCR products were 1865 base pair.

Tables

Table 1. The result of Jonckheere-Terpstra test of wild-type cells treated with vanillin.

rank	Parameter	Description	Z value	P value	Q value
1	D145_A1B	Distance_between_nuclear_outline_point_D7_and_mother_hip	-4.32673	1.51E-05	0.004994
2	D104_A1B	Distance_between_nuclear_gravity_center_and_mother_tip	-3.89645	9.76E-05	0.010738
3	D152_A1B	Mobility_of_nucleus_in_mother	3.896445	9.76E-05	0.010738
4	D126_A1B	Distance_between_nuclear_gravity_center_and_mother_hip	-3.80083	0.000144	0.011898
5	D142_A1B	Distance_between_nuclear_brightest_point_and_mother_hip	-3.51397	0.000441	0.029136
6	C128_A1B	Distance_between_middle_point_of_neck_and_mother_hip	-3.41835	0.00063	0.034651
7	C112_A1B	Distance_between_middle_point_of_neck_and_mother_center	-3.27493	0.001057	0.037475
8	C101_A1B	Whole_cell_size	-3.22712	0.00125	0.037475
9	D129_A1B	Distance_between_nuclear_brightest_point_and_mother_tip	-3.22712	0.00125	0.037475
10	DCV116_C	CV_of_Distance_between_two_nuclear_gravity_centers_through_middle_point_of_neck	3.227117	0.00125	0.037475
11	DCV134_C	CV_of_Distance_between_two_nuclear_brightest_points_through_middle_point_of_neck	3.227117	0.00125	0.037475
12	DCV108_C	CV_of_Distance_between_nuclear_gravity_center_in_mother_and_middle_point_of_neck	3.179308	0.001476	0.037475
13	DCV143_C	CV_of_Distance_between_nuclear_outline_point_D6-1_in_mother_and_middle_point_of_neck	3.179308	0.001476	0.037475
14	DCV130_C	CV_of_Distance_between_nuclear_brightest_point_in_mother_and_middle_point_of_neck	3.08369	0.002045	0.04397
15	A7-1_A	Size_of_actin_region	-3.03588	0.002398	0.04397
16	D118_A1B	Distance_between_nuclear_gravity_center_and_mother_center	-3.03588	0.002398	0.04397
17	D134_C	Distance_between_two_nuclear_brightest_points_through_middle_point_of_neck	-3.03588	0.002398	0.04397
18	DCV112_C	CV_of_Ratio_of_D108_to_C128	3.035881	0.002398	0.04397
19	C11-1_A	Whole_cell_size	-2.89245	0.003822	0.063071
20	C103_A	Long_axis_length_in_whole_cell	-2.89245	0.003822	0.063071
21	C104_A	Short_axis_length_in_whole_cell	-2.84464	0.004446	0.069867
22	C104_A1B	Short_axis_length_in_mother	-2.79683	0.005161	0.077409
23	C12-1_A	Whole_cell_outline_length	-2.74903	0.005977	0.0789
24	C11-1_A1B	Mother_cell_size	-2.74903	0.005977	0.0789
25	C12-1_A1B	Mother_cell_outline_length	-2.74903	0.005977	0.0789
26	C103_A1B	Long_axis_length_in_mother	-2.70122	0.006909	0.081423
27	D107_A1B	Ratio_of_D104_to_C103	-2.70122	0.006909	0.081423
28	C112_C	Distance_between_middle_point_of_neck_and_mother_center	-2.70122	0.006909	0.081423
29	C102_A1B	Whole_cell_outline_length	-2.65341	0.007968	0.087652
30	C109_A1B	Neck_width	-2.65341	0.007968	0.087652
31	D102_A	Distance_between_nuclear_gravity_center_and_mother_tip	-2.6056	0.009171	0.088541
32	D127_A	Distance_between_nuclear_brightest_point_and_cell_tip	-2.6056	0.009171	0.088541
33	D130_C	Distance_between_nuclear_brightest_point_in_mother_and_middle_point_of_neck	-2.6056	0.009171	0.088541
34	D143_C	Distance_between_nuclear_outline_point_D6-1_in_mother_and_middle_point_of_neck	-2.6056	0.009171	0.088541
35	A9_A1B	Proportion_of_actin_region_at_neck	-2.55779	0.010534	0.088541
36	D136_A1B	Distance_between_nuclear_brightest_point_and_mother_center	-2.55779	0.010534	0.088541
37	D108_C	Distance_between_nuclear_gravity_center_in_mother_and_middle_point_of_neck	-2.55779	0.010534	0.088541
38	DCV131_C	CV_of_Distance_between_nuclear_brightest_point_in_bud_and_middle_point_of_neck	2.557789	0.010534	0.088541
39	DCV151_C	CV_of_Ratio_of_distance_between_each_nucleus_and_middle_point_of_neck	2.557789	0.010534	0.088541
40	D117_A	Distance_between_nuclear_gravity_center_and_cell_center	-2.50998	0.012074	0.088541
41	D114_A1B	Ratio_of_D110_to_C128	2.50998	0.012074	0.088541
42	C104_C	Short_axis_length_in_mother	-2.50998	0.012074	0.088541
43	C118_C	Cell_size_ratio	2.50998	0.012074	0.088541
44	ACV103_C	CV_of_Relative_distance_of_actin_patch_center_from_neck_in_mother	-2.50998	0.012074	0.088541
45	DCV176_C	CV_of_Nuclear_long_axis_length_in_mother	2.50998	0.012074	0.088541
46	D17-1_A	Nuclear_fitness_for_ellipse	2.48726	0.012873	0.089358
47	A8-1_A	Actin_region_brightness	-2.46217	0.01381	0.089358
48	C111_A1B	Distance_between_bud_tip_and_mother_short_axis_extension	-2.46217	0.01381	0.089358
49	C125_A1B	Large_bud_ratio	2.462171	0.01381	0.089358
50	C128_C	Distance_between_middle_point_of_neck_and_mother_hip	-2.46217	0.01381	0.089358
51	DCV173_C	CV_of_Maximal_distance_between_nuclear_gravity_center_and_nuclear_outline_in_mother	2.462171	0.01381	0.089358
52	A102_C	Bud_actin_region_ratio_to_total_region	-2.41436	0.015763	0.100033
53	C11-1_C	Mother_cell_size	-2.36655	0.017955	0.107728
54	C109_C	Neck_width	-2.36655	0.017955	0.107728
55	A8-2_C	Total_brightness_of_actin_region_in_bud	-2.36655	0.017955	0.107728
56	DCV127_A	CV_of_Distance_between_nuclear_brightest_point_and_cell_tip	-2.31874	0.020409	0.114152
57	C108_A1B	Short_axis_length_in_bud	-2.31874	0.020409	0.114152
58	C103_C	Long_axis_length_in_mother	-2.31874	0.020409	0.114152
59	DCV113_C	CV_of_Ratio_of_D109_to_C107	2.318744	0.020409	0.114152

Table 1. (continued)

rank	Parameter	Description	Z value	P value	Q value
60	C106_A1B	Bud_direction	2.270934	0.023151	0.125243
61	DCV139_C	CV_of_Distance_between_nuclear_brightest_point_in_bud_and_bud_tip	2.270934	0.023151	0.125243
62	C13_A	Whole_cell_fitness_for_ellipse	2.224185	0.026136	0.131037
63	CCV110_A1B	CV_of_Distance_between_bud_tip_and_mother_long_axis_extension	-2.22313	0.026207	0.131037
64	C101_C	Whole_cell_size	-2.22313	0.026207	0.131037
65	DCV109_C	CV_of_Distance_between_nuclear_gravity_center_in_bud_and_middle_point_of_neck	2.223125	0.026207	0.131037
66	DCV121_C	CV_of_Distance_between_nuclear_gravity_center_in_bud_and_bud_tip	2.223125	0.026207	0.131037
67	C124_A1B	Medium_bud_ratio	-2.17532	0.029606	0.141596
68	DCV110_A1B	CV_of_Distance_between_nuclear_gravity_center_and_middle_point_of_neck	-2.17532	0.029606	0.141596
69	DCV114_A1B	CV_of_Ratio_of_D110_to_C128	-2.17532	0.029606	0.141596
70	A8-1_A1B	Total_brightness_of_actin_region_in_mother	-2.12751	0.033378	0.148848
71	C12-1_C	Mother_cell_outline_length	-2.12751	0.033378	0.148848
72	D116_C	Distance_between_two_nuclear_gravity_centers_through_middle_point_of_neck	-2.12751	0.033378	0.148848
73	ACV101_C	CV_of_Actin_region_ratio_in_whole_cell	2.127507	0.033378	0.148848
74	DCV123_C	CV_of_Ratio_of_D121_to_C107	2.127507	0.033378	0.148848
75	C127_C	Thickness_difference_of_cell_wall	-2.08069	0.037462	0.156868
76	A8-2_A1B	Total_brightness_of_actin_region_in_bud	-2.0797	0.037553	0.156868
77	CCV105_A1B	CV_of_Neck_position	-2.0797	0.037553	0.156868
78	CCV106_A1B	CV_of_Bud_direction	-2.0797	0.037553	0.156868
79	C117_C	Cell_outline_ratio	2.079698	0.037553	0.156868
80	DCV105_A	CV_of_Ratio_of_D102_to_C103	-2.03189	0.042165	0.165648
81	D112_C	Ratio_of_D108_to_C128	-2.03189	0.042165	0.165648
82	CCV116_C	CV_of_Axis_ratio_ratio	2.031889	0.042165	0.165648
83	DCV144_C	CV_of_Distance_between_nuclear_outline_point_D6-2_in_bud_and_middle_point_of_neck	2.031889	0.042165	0.165648
84	D207	nuclear_A1_ratio_to_budded_cells	2.031889	0.042165	0.165648
85	A120_C	Total_length_of_actin_patch_link	-1.98408	0.047247	0.181297
86	D163_C	Angle_between_D2-1D2-2_and_C1C4-1	1.984079	0.047247	0.181297
87	A121_A	Maximal_distance_between_patches	-1.93627	0.052835	0.187478
88	A7-2_A1B	Size_of_actin_region_in_bud	-1.93627	0.052835	0.187478
89	A121_A1B	Maximal_distance_between_patches	-1.93627	0.052835	0.187478
90	D170_A1B	Angle_between_C4-1D2-1_and_C4-1C1	1.93627	0.052835	0.187478
91	A121_C	Maximal_distance_between_patches	-1.93627	0.052835	0.187478
92	ACV123_C	CV_of_Ratio_of_actin_patches_to_actin_region	-1.93627	0.052835	0.187478
93	DCV195_C	CV_of_Maximal_intensity_of_nuclear_brightness_divided_by_average_in_bud	-1.93627	0.052835	0.187478
94	A120_A	Total_length_of_actin_patch_link	-1.88846	0.058964	0.198552
95	A103_A1B	Relative_distance_of_actin_patch_center_from_neck_in_mother	1.888461	0.058964	0.198552
96	D186_C	Total_length_of_two_straight_segments_D12-1C4-1_and_D12-2C4-1	-1.88846	0.058964	0.198552
97	CCV115_C	CV_of_Mother_axis_ratio	1.888461	0.058964	0.198552
98	D214	nuclear_A1_ratio_to_nuclear_A1BC_cells	1.888461	0.058964	0.198552

Details of parameters presented are available in SCMD (http://yeast.gi.k.u-tokyo.ac.jp/datamine/).

Table 2. Gene ontology terms detected in the inference result of wild-type cells. Each symbol means any enrichment was detected under P value < 0.01 and ND means not detected. Below table shows details of the GO terms.

Rank in the 4718 mutants	WT (*his3*Δ)					
	Inference Results			GO term		
	R value	P value	Q value	Process	Function	Component
10	0.519516	1.60E-08	8.74E-07	ND	ND	ND
20	0.496973	8.04E-08	2.55E-06	ND	ND	ND
30	0.47189	4.26E-07	9.19E-06	ND	ND	**a**
40	0.453173	1.36E-06	2.22E-05	ND	ND	ND
50	0.444994	2.21E-06	3.12E-05	ND	ND	ND
60	0.439587	3.03E-06	3.68E-05	ND	ND	ND
70	0.432225	4.61E-06	5.10E-05	ND	ND	ND
80	0.428863	5.57E-06	5.79E-05	ND	ND	**b**
90	0.418614	9.77E-06	9.34E-05	ND	ND	**c**
100	0.413898	1.26E-05	1.12E-04	ND	ND	**d**
150	0.383402	5.89E-05	3.76E-04	ND	ND	ND
200	0.367393	1.25E-04	6.55E-04	ND	ND	ND
300	0.337769	4.54E-04	0.001666	ND	ND	ND
400	0.311226	0.001301	0.003636	ND	ND	ND
500	0.289931	0.002832	0.006353	ND	ND	ND

	GO_term	Cluster frequency	Background frequency	P-value	FDR	Expected FP	Genes annotated to the term
a	**large ribosomal subunit**	6 out of 30 genes, 20.0%	109 out of 4707 background genes, 2.3%	0.00203	0	0	RPL19A/YBR084C-A:RPP2B/YDR382W:RPL16A/YIL133C:MRPL31/YKL138C:RPL36A/YMR194W:RPL9B/YNL067W
	cytosolic large ribosomal subunit	5 out of 30 genes, 16.7%	67 out of 4707 background genes, 1.4%	0.00217	0	0	RPL19A/YBR084C-A:RPP2B/YDR382W:RPL16A/YIL133C:RPL36A/YMR194W:RPL9B/YNL067W
b	**cytosolic large ribosomal subunit**	7 out of 80 genes, 8.8%	67 out of 4707 background genes, 1.4%	0.00878	0	0	RPL23A/YBL087C:RPL19A/YBR084C-A:RPP2B/YDR382W:RPL9A/YGL147C:RPL16A/YIL133C:RPL36A/YMR194W:RPL9B/YNL067W
c	**cytosolic large ribosomal subunit**	9 out of 90 genes, 10.0%	67 out of 4707 background genes, 1.4%	0.00032	0	0	RPL23A/YBL087C:RPL19A/YBR084C-A:RPP2B/YDR382W:RPL7A/YGL076C:RPL9A/YGL147C:RPL8A/YHL033C:RPL16A/YIL133C:RPL36A/YMR194W:RPL9B/YNL067W
	large ribosomal subunit	11 out of 90 genes, 12.2%	109 out of 4707 background genes, 2.3%	0.00045	0	0	MRPL16/YBL038W:RPL23A/YBL087C:RPL19A/YBR084C-A:RPP2B/YDR382W:RPL7A/YGL076C:RPL9A/YGL147C:RPL8A/YHL033C:RPL16A/YIL133C:MRPL31/YKL138C:RPL36A/YMR194W:RPL9B/YNL067W
d	**cytosolic large ribosomal subunit**	9 out of 100 genes, 9.0%	67 out of 4707 background genes, 1.4%	0.00082	0	0	RPL23A/YBL087C:RPL19A/YBR084C-A:RPP2B/YDR382W:RPL7A/YGL076C:RPL9A/YGL147C:RPL8A/YHL033C:RPL16A/YIL133C:RPL36A/YMR194W:RPL9B/YNL067W
	large ribosomal subunit	11 out of 100 genes, 11.0%	109 out of 4707 background genes, 2.3%	0.00136	0	0	MRPL16/YBL038W:RPL23A/YBL087C:RPL19A/YBR084C-A:RPP2B/YDR382W:RPL7A/YGL076C:RPL9A/YGL147C:RPL8A/YHL033C:RPL16A/YIL133C:MRPL31/YKL138C:RPL36A/YMR194W:RPL9B/YNL067W

Table 3. The result of Jonckheere-Terpstra test of *erg6*Δ treated with vanillin.

rank	Paarameter	Description	Z value	P value	Q value
1	D145_A1B	Distance_between_nuclear_outline_point_D7_and_mother_hip	-4.13549	3.54E-05	0.006004
2	DCV147_A1B	CV_of_Relative_distance_of_nuclear_gravity_center_to_mother_center	3.992064	6.55E-05	0.006004
3	DCV148_A1B	CV_of_Relative_distance_of_nuclear_brightest_point_to_mother_center	3.992064	6.55E-05	0.006004
4	D152_A1B	Mobility_of_nucleus_in_mother	3.848636	1.19E-04	0.007932
5	DCV118_A1B	CV_of_Distance_between_nuclear_gravity_center_and_mother_center	3.800827	1.44E-04	0.007932
6	C112_A1B	Distance_between_middle_point_of_neck_and_mother_center	-3.70521	2.11E-04	0.008298
7	D129_A1B	Distance_between_nuclear_brightest_point_and_mother_tip	-3.70521	2.11E-04	0.008298
8	C115_A	Whole_cell_axis_ratio	-3.51397	4.41E-04	0.01214
9	D104_A1B	Distance_between_nuclear_gravity_center_and_mother_tip	-3.56178	3.68E-04	0.01214
10	D142_A1B	Distance_between_nuclear_brightest_point_and_mother_hip	-3.51397	4.41E-04	0.01214
11	D17-1_A	Nuclear_fitness_for_ellipse	3.418354	6.30E-04	0.012375
12	C111_A1B	Distance_between_bud_tip_and_mother_short_axis_extension	-3.46616	5.28E-04	0.012375
13	D114_A1B	Ratio_of_D110_to_C128	3.418354	6.30E-04	0.012375
14	D147_A1B	Relative_distance_of_nuclear_gravity_center_to_mother_center	-3.41835	6.30E-04	0.012375
15	D126_A1B	Distance_between_nuclear_gravity_center_and_mother_hip	-3.37054	7.50E-04	0.013754
16	D118_A1B	Distance_between_nuclear_gravity_center_and_mother_center	-3.32274	8.91E-04	0.01442
17	D144_C	Distance_between_nuclear_outline_point_D6-2_in_bud_and_middle_point_of_neck	-3.32274	8.91E-04	0.01442
18	D117_A	Distance_between_nuclear_gravity_center_and_cell_center	-3.27493	0.001057	0.016147
19	D107_A1B	Ratio_of_D104_to_C103	-3.22712	0.00125	0.016375
20	DCV136_A1B	CV_of_Distance_between_nuclear_brightest_point_and_mother_center	3.227117	0.00125	0.016375
21	C112_C	Distance_between_middle_point_of_neck_and_mother_center	-3.22712	0.00125	0.016375
22	C128_A1B	Distance_between_middle_point_of_neck_and_mother_hip	-3.17931	0.001476	0.018453
23	DCV17-1_A	CV_of_Nuclear_fitness_for_ellipse	3.131499	0.001739	0.019131
24	C103_A1B	Long_axis_length_in_mother	-3.1315	0.001739	0.019131
25	D116_C	Distance_between_two_nuclear_gravity_centers_through_middle_point_of_neck	-3.1315	0.001739	0.019131
26	D108_C	Distance_between_nuclear_gravity_center_in_mother_and_middle_point_of_neck	-3.08369	0.002045	0.02008
27	D134_C	Distance_between_two_nuclear_brightest_points_through_middle_point_of_neck	-3.08369	0.002045	0.02008
28	DCV143_C	CV_of_Distance_between_nuclear_outline_point_D6-1_in_mother_and_middle_point_of_neck	3.08369	0.002045	0.02008
29	DCV14-3_A1B	CV_of_Nuclear_size	3.035881	0.002398	0.021985
30	C103_C	Long_axis_length_in_mother	-3.03588	0.002398	0.021985
31	D147_A	Relative_distance_of_nuclear_gravity_center_to_cell_center	-2.98807	0.002807	0.022707
32	D131_C	Distance_between_nuclear_brightest_point_in_bud_and_middle_point_of_neck	-2.98807	0.002807	0.022707
33	D143_C	Distance_between_nuclear_outline_point_D6-1_in_mother_and_middle_point_of_neck	-2.98807	0.002807	0.022707
34	DCV15-2_C	CV_of_Nuclear_brightness_in_bud	2.988072	0.002807	0.022707
35	ACV8-1_A	CV_of_Actin_region_brightness	-2.89245	0.003822	0.029199
36	A110_C	Actin_f_ratio	-2.89383	0.003806	0.029199
37	D102_A	Distance_between_nuclear_gravity_center_and_mother_tip	-2.84464	0.004446	0.032176
38	C12-1_A1B	Mother_cell_outline_length	-2.84464	0.004446	0.032176
39	C103_A	Long_axis_length_in_whole_cell	-2.79683	0.005161	0.035479
40	DCV177_C	CV_of_Nuclear_long_axis_length_in_bud	2.796835	0.005161	0.035479
41	D17-1_C	Nuclear_fitness_for_ellipse_in_mother	2.749026	0.005977	0.039137
42	DCV174_C	CV_of_Maximal_distance_between_nuclear_gravity_center_and_nuclear_outline_in_bud	2.749026	0.005977	0.039137
43	C11-1_A1B	Mother_cell_size	-2.70122	0.006909	0.042219
44	D112_C	Ratio_of_D108_to_C128	-2.70122	0.006909	0.042219
45	D186_C	Total_length_of_two_straight_segments_D12-1C4-1_and_D12-2C4-1	-2.70122	0.006909	0.042219
46	DCV173_A	CV_of_Maximal_distance_between_nuclear_gravity_center_and_nuclear_outline	2.653408	0.007968	0.045652
47	C12-1_C	Mother_cell_outline_length	-2.65341	0.007968	0.045652
48	A106	actin_b_ratio	-2.65341	0.007968	0.045652
49	ACV7-1_A	CV_of_Size_of_actin_region	-2.6056	0.009171	0.049454
50	D148_A1B	Relative_distance_of_nuclear_brightest_point_to_mother_center	-2.6056	0.009171	0.049454
51	D152_C	Mobility_of_nucleus_in_mother	-2.6056	0.009171	0.049454
52	C125_A1B	Large_bud_ratio	2.559008	0.010497	0.053645
53	D109_C	Distance_between_nuclear_gravity_center_in_bud_and_middle_point_of_neck	-2.55779	0.010534	0.053645
54	D130_C	Distance_between_nuclear_brightest_point_in_mother_and_middle_point_of_neck	-2.55779	0.010534	0.053645
55	ACV101_A	CV_of_Actin_region_ratio_in_whole_cell	-2.50998	0.012074	0.058251
56	C128_C	Distance_between_middle_point_of_neck_and_mother_hip	-2.50998	0.012074	0.058251
57	DCV144_C	CV_of_Distance_between_nuclear_outline_point_D6-2_in_bud_and_middle_point_of_neck	2.50998	0.012074	0.058251
58	A105_A	Actin_a_ratio	2.462171	0.01381	0.062258
59	A121_A	Maximal_distance_between_patches	-2.46217	0.01381	0.062258
60	D136_A1B	Distance_between_nuclear_brightest_point_and_mother_center	-2.46217	0.01381	0.062258
61	C102_C	Whole_cell_outline_length	-2.46217	0.01381	0.062258
62	A106_A	Actin_b_ratio	-2.41436	0.015763	0.066689
63	DCV155_A1B	CV_of_Angle_between_C1D2-1_and_C1C1-2	-2.41436	0.015763	0.066689
64	C107_C	Long_axis_length_in_bud	-2.41436	0.015763	0.066689
65	DCV125_C	CV_of_Distance_between_nuclear_gravity_center_in_mother_and_mother_hip	-2.41436	0.015763	0.066689
66	D17-3_A1B	Nuclear_fitness_for_ellipse	2.366553	0.017955	0.071558
67	DCV145_A1B	CV_of_Distance_between_nuclear_outline_point_D7_and_mother_hip	2.366553	0.017955	0.071558
68	D185_C	Total_length_of_two_straight_segments_D11-1C4-1_and_D11-2C4-1	-2.36655	0.017955	0.071558
69	DCV14-2_C	CV_of_Nuclear_size_in_bud	2.366553	0.017955	0.071558
70	C101_A1B	Whole_cell_size	-2.31874	0.020409	0.076883
71	CCV111_A1B	CV_of_Distance_between_bud_tip_and_mother_short_axis_extension	2.318744	0.020409	0.076883
72	DCV181_A1B	CV_of_Nuclear_minimum_radius	2.318744	0.020409	0.076883
73	DCV162_C	CV_of_Angle_between_D1-1D1-2_and_C1C4-1	2.318744	0.020409	0.076883
74	D127_A	Distance_between_nuclear_brightest_point_and_cell_tip	-2.27093	0.023151	0.08377
75	DCV147_A	CV_of_Relative_distance_of_nuclear_gravity_center_to_cell_center	2.270934	0.023151	0.08377
76	D153_C	Mobility_of_nucleus_in_bud	-2.27093	0.023151	0.08377
77	A113	actin_n_ratio	2.256628	0.024031	0.085826

Table 3. (contineued)

rank	Paarameter	Description	Z value	P value	Q value
78	C102_A1B	Whole_cell_outline_length	-2.22313	0.026207	0.088976
79	DCV161_A1B	CV_of_Angle_between_D3-1D4-1_and_C1-1C1-2_or_between_D3-3D4-3_and_C1-1C1-2	2.223125	0.026207	0.088976
80	D113_C	Ratio_of_D109_to_C107	-2.22313	0.026207	0.088976
81	ACV101_C	CV_of_Actin_region_ratio_in_whole_cell	-2.22313	0.026207	0.088976
82	C12-1_A	Whole_cell_outline_length	-2.17532	0.029606	0.090464
83	DCV188_A	CV_of_Distance_between_nuclear_gravity_center_and_brightest_point	2.175316	0.029606	0.090464
84	DCV194_A	CV_of_Maximal_intensity_of_nuclear_brightness_divided_by_average	2.175316	0.029606	0.090464
85	C104_A1B	Short_axis_length_in_mother	-2.17532	0.029606	0.090464
86	DCV129_A1B	CV_of_Distance_between_nuclear_brightest_point_and_mother_tip	2.175316	0.029606	0.090464
87	A122_C	Number_of_bright_actin_patches	2.176353	0.029529	0.090464
88	DCV141_C	CV_of_Distance_between_nuclear_brightest_point_in_mother_and_mother_hip	-2.17532	0.029606	0.090464
89	A114	actin_a_ratio_to_no_bud_cells	2.199744	0.027825	0.090464
90	A115	actin_b_ratio_to_no_bud_cells	-2.19974	0.027825	0.090464
91	A119	actin_f_ratio_to_budded_cells	-2.15192	0.031403	0.0949
92	C11-1_A	Whole_cell_size	-2.12751	0.033378	0.09662
93	C101_C	Whole_cell_size	-2.12751	0.033378	0.09662
94	C115_C	Mother_axis_ratio	-2.12751	0.033378	0.09662
95	D123_C	Ratio_of_D121_to_C107	2.127507	0.033378	0.09662
96	D182_A	Nuclear_axis_ratio	2.079698	0.037553	0.104315
97	C11-1_C	Mother_cell_size	-2.0797	0.037553	0.104315
98	D182_C	Nuclear_axis_ratio_in_mother	2.079698	0.037553	0.104315
99	DCV180_C	CV_of_Nuclear_minimum_radius_in_bud	2.079698	0.037553	0.104315
100	A113_A	Actin_n_ratio	2.06451	0.038969	0.107166
101	A121_C	Maximal_distance_between_patches	-2.03189	0.042165	0.112576
102	D166_C	Angle_between_D1-1D1-2_and_C4-1C4-2	2.031889	0.042165	0.112576
103	DCV176_C	CV_of_Nuclear_long_axis_length_in_mother	2.031889	0.042165	0.112576
104	C113_C	Distance_between_bud_tip_and_mother_long_axis_through_middle_point_of_neck	-1.98408	0.047247	0.122575
105	ACV102_C	CV_of_Bud_actin_region_ratio_to_total_region	1.984079	0.047247	0.122575
106	DCV195_C	CV_of_Maximal_intensity_of_nuclear_brightness_divided_by_average_in_bud	1.984079	0.047247	0.122575
107	D172_A1B	Angle_between_C4-1D4_and_C4-1C1	1.93627	0.052835	0.134533
108	D211	nuclear_A1_ratio_to_nuclear_AA1BC_cells	1.93627	0.052835	0.134533
109	DCV104_A1B	CV_of_Distance_between_nuclear_gravity_center_and_mother_tip	1.888461	0.058964	0.14741
110	DCV142_A1B	CV_of_Distance_between_nuclear_brightest_point_and_mother_hip	1.888461	0.058964	0.14741
111	A101_A	Actin_region_ratio_in_whole_cell	1.840652	0.065673	0.157043
112	D132_A1B	Distance_between_nuclear_brightest_point_and_middle_point_of_neck	1.840652	0.065673	0.157043
113	ACV103_A1B	CV_of_Relative_distance_of_actin_patch_center_from_neck_in_mother	-1.84065	0.065673	0.157043
114	DCV107_A1B	CV_of_Ratio_of_D104_to_C103	1.840652	0.065673	0.157043
115	DCV197_C	CV_of_Ratio_of_nuclear_size	1.840652	0.065673	0.157043
116	DCV176_A	CV_of_Nuclear_long_axis_length	1.792843	0.072998	0.164545
117	ACV8-1_A1B	CV_of_Total_brightness_of_actin_region_in_mother	1.792843	0.072998	0.164545
118	C110_C	Distance_between_bud_tip_and_mother_long_axis_extension	-1.79284	0.072998	0.164545
119	D198_C	Ratio_of_nuclear_brightness	1.792843	0.072998	0.164545
120	DCV103_C	CV_of_Distance_between_nuclear_gravity_center_in_mother_and_mother_tip	-1.79284	0.072998	0.164545
121	A110	actin_f_ratio	-1.79284	0.072998	0.164545
122	D200	nuclear_A1_ratio	1.792843	0.072998	0.164545
123	D155_A1B	Angle_between_C1D2-1_and_C1C1-2	1.745034	0.080979	0.17674
124	ACV104_C	CV_of_Relative_distance_of_actin_patch_center_from_neck_in_bud	-1.74503	0.080979	0.17674
125	DCV123_C	CV_of_Ratio_of_D121_to_C107	-1.74503	0.080979	0.17674
126	DCV198_C	CV_of_Ratio_of_nuclear_brightness	1.745034	0.080979	0.17674
127	D154_A	Angle_between_C1D1-1_and_C1C1-2	-1.69722	0.089654	0.188205
128	CCV126_A1B	CV_of_Brightness_difference_of_cell_wall	1.697225	0.089654	0.188205
129	ACV122_A1B	CV_of_Number_of_bright_actin_patches	1.697225	0.089654	0.188205
130	DCV15-1_C	CV_of_Nuclear_brightness_in_mother	1.697225	0.089654	0.188205
131	DCV146_C	CV_of_Distance_between_nuclear_outline_point_D8_in_bud_and_bud_tip	-1.69722	0.089654	0.188205

Details of parameters presented are available in SCMD (http://yeast.gi.k.u-tokyo.ac.jp/datamine/).

Table 4. Gene ontology terms detected in the inference result of *erg6*Δ.
Each symbol means any enrichment is detected under P value < 0.01 and ND means not detected. Below table shows details of the GO terms.

Rank in the 4718 mutants	*erg6*Δ					
	Inference Results			GO term		
	R value	P value	Q value	Process	Function	Component
10	0.564441	4.37E-10	5.61E-08	ND	ND	ND
20	0.539757	3.37E-09	2.40E-07	ND	ND	ND
30	0.5169	1.94E-08	8.11E-07	ND	ND	**a**
40	0.494269	9.69E-08	3.03E-06	ND	ND	ND
50	0.480033	2.52E-07	6.22E-06	ND	ND	**b**
60	0.467679	5.57E-07	1.02E-05	ND	ND	**c**
70	0.456809	1.09E-06	1.72E-05	ND	**d**	**e**
80	0.447721	1.88E-06	2.55E-05	ND	**f**	**g**
90	0.442384	2.58E-06	3.16E-05	**h**	**i**	**j**
100	0.43187	4.70E-06	5.04E-05	**k**	ND	**l**
150	0.40031	2.55E-05	1.75E-04	**m**	ND	**n**
200	0.374826	8.85E-05	4.36E-04	ND	**o**	**p**
300	0.339502	4.22E-04	0.001345	ND	ND	**q**
400	0.302177	0.001823	0.004217	ND	ND	**r**
500	0.277472	0.004349	0.008198	ND	ND	**s**

	GO_term	Cluster frequency	Background frequency	P-value	FDR	Expected FP	Genes annotated to the term
a	**cytosolic large ribosomal subunit**	5 out of 30 genes, 16.7%	67 out of 4707 background genes, 1.4%	0.00239	0	0	RPL19A/YBR084C-A, RPL31A/YDL075W, RPP2B/YDR382W, RPL22A/YLR061W, RPL36A/YMR194W
b	**large ribosomal subunit**	8 out of 50 genes, 16.0%	109 out of 4707 background genes, 2.3%	0.00118	0	0	RPL23A/YBL087C:RPL19A/YBR084C-A:RPL31A/YDL075W:MRPL1/YDR116C:RPP2B/YDR382W:RPL22A/YLR061W:MRPL24/YMR193W:RPL36A/YMR194W
	cytosolic large ribosomal subunit	6 out of 50 genes, 12.0%	67 out of 4707 background genes, 1.4%	0.00496	0	0	RPL23A/YBL087C:RPL19A/YBR084C-A:RPL31A/YDL075W:RPP2B/YDR382W:RPL22A/YLR061W:RPL36A/YMR194W
c	**large ribosomal subunit**	9 out of 60 genes, 15.0%	109 out of 4707 background genes, 2.3%	0.00065	0	0	RPL23A/YBL087C:RPL19A/YBR084C-A:RPL31A/YDL075W:MRPL1/YDR116C:RPP2B/YDR382W:RPL22A/YLR061W:RPL37A/YLR185W:MRPL24/YMR193W:RPL36A/YMR194W
	cytosolic large ribosomal subunit	7 out of 60 genes, 11.7%	67 out of 4707 background genes, 1.4%	0.00157	0	0	RPL23A/YBL087C:RPL19A/YBR084C-A:RPL31A/YDL075W:RPP2B/YDR382W:RPL22A/YLR061W:RPL37A/YLR185W:RPL36A/YMR194W
	cytosolic part	10 out of 60 genes, 16.7%	157 out of 4707 background genes, 3.3%	0.00197	0	0	RPL23A/YBL087C:RPL19A/YBR084C-A:RPL31A/YDL075W:RPP2B/YDR382W:RPL22A/YLR061W:PEP3/YLR148W:RPL37A/YLR185W:VPS34/YLR240W:RPN13/YLR421C:RPL36A/YMR194W
	macromolecular complex	27 out of 60 genes, 45.0%	1075 out of 4707 background genes, 22.8%	0.00956	0	0	RPL23A/YBL087C:RPL19A/YBR084C-A:RPL31A/YDL075W:OST4/YDL232W:MRPL1/YDR116C:RPP2B/YDR382W:PAC11/YDR488C:LOC1/YFR001W:MIP6/YHR015W:RAV1/YJR033C:TEF4/YKL081W:SAC1/YKL212W:PAM17/YKR065C:RPL22A/YLR061W:PEP3/YLR148W:RPL37A/YLR185W:VPS34/YLR240W:RPN13/YLR421C:MRPL24/YMR193W:RPL36A/YMR194W:PEP5/YMR231W:COX7/YMR256C:JNM1/YMR294W:TOP1/YOL006C:SSN3/YPL042C:HOS1/YPR068C:MED1/YPR070W
d	**structural constituent of ribosome**	10 out of 70 genes, 14.3%	178 out of 4707 background genes, 3.8%	0.00898	0.08	0.08	RPL23A/YBL087C:RPL19A/YBR084C-A:RPL31A/YDL075W:MRPL1/YDR116C:RPP2B/YDR382W:RPL22A/YLR061W:RPL37A/YLR185W:MRPL24/YMR193W:RPL36A/YMR194W:MRPL44/YMR225C
e	**large ribosomal subunit**	10 out of 70 genes, 14.3%	109 out of 4707 background genes, 2.3%	0.00035	0	0	RPL23A/YBL087C:RPL19A/YBR084C-A:RPL31A/YDL075W:MRPL1/YDR116C:RPP2B/YDR382W:RPL22A/YLR061W:MRPL24/YMR193W:RPL36A/YMR194W:MRPL44/YMR225C
	cytosolic large ribosomal subunit	7 out of 70 genes, 10.0%	67 out of 4707 background genes, 1.4%	0.00493	0	0	RPL23A/YBL087C:RPL19A/YBR084C-A:RPL31A/YDL075W:RPP2B/YDR382W:RPL22A/YLR061W:RPL37A/YLR185W:RPL36A/YMR194W
	cytosolic part	10 out of 70 genes, 14.3%	157 out of 4707 background genes, 3.3%	0.00878	0	0	RPL23A/YBL087C:RPL19A/YBR084C-A:RPL31A/YDL075W:RPP2B/YDR382W:RPL22A/YLR061W:PEP3/YLR148W:RPL37A/YLR185W:VPS34/YLR240W:RPN13/YLR421C:RPL36A/YMR194W
f	**structural constituent of ribosome**	11 out of 80 genes, 13.8%	178 out of 4707 background genes, 3.8%	0.00661	0.02	0.02	RPL23A/YBL087C:RPL19A/YBR084C-A:RPL31A/YDL075W:MRPL1/YDR116C:RPP2B/YDR382W:RPL22A/YLR061W:RPL37A/YLR185W:MRPL24/YMR193W:RPL36A/YMR194W:MRPL44/YMR225C:RPL20A/YMR242C
g	**large ribosomal subunit**	11 out of 80 genes, 13.8%	109 out of 4707 background genes, 2.3%	0.00016	0	0	RPL23A/YBL087C:RPL19A/YBR084C-A:RPL31A/YDL075W:MRPL1/YDR116C:RPP2B/YDR382W:RPL22A/YLR061W:RPL37A/YLR185W:MRPL24/YMR193W:RPL36A/YMR194W:MRPL44/YMR225C:RPL20A/YMR242C
	cytosolic large ribosomal subunit	8 out of 80 genes, 10.0%	67 out of 4707 background genes, 1.4%	0.00137	0	0	RPL23A/YBL087C:RPL19A/YBR084C-A:RPL31A/YDL075W:RPP2B/YDR382W:RPL22A/YLR061W:RPL37A/YLR185W:RPL36A/YMR194W:RPL20A/YMR242C
	cytosolic part	11 out of 80 genes, 13.8%	157 out of 4707 background genes, 3.3%	0.00557	0	0	RPL23A/YBL087C:RPL19A/YBR084C-A:RPL31A/YDL075W:RPP2B/YDR382W:RPL22A/YLR061W:PEP3/YLR148W:RPL37A/YLR185W:VPS34/YLR240W:RPN13/YLR421C:RPL36A/YMR194W:RPL20A/YMR242C
h	**vesicle fusion**	5 out of 90 genes, 5.6%	18 out of 4707 background genes, 0.4%	0.0047	0	0	GOS1/YHL031C:PEP3/YLR148W:PEP5/YMR231W:VAM3/YOR106W:SNC2/YOR327C
i	**structural constituent of ribosome**	12 out of 90 genes, 13.3%	178 out of 4707 background genes, 3.8%	0.00527	0	0	RPL23A/YBL087C:RPL19A/YBR084C-A:RPL31A/YDL075W:MRPL1/YDR116C:RPP2B/YDR382W:RPL7A/YGL076C:RPL22A/YLR061W:RPL37A/YLR185W:MRPL24/YMR193W:RPL36A/YMR194W:MRPL44/YMR225C:RPL20A/YMR242C

Table 4. (contineued)

	GO_term	Cluster frequency	Background frequency	P-value	FDR	Expected FP	Genes annotated to the term
j	**large ribosomal subunit**	13 out of 90 genes, 14.4%	109 out of 4707 background genes, 2.3%	0.00001	0	0	RPL23A/YBL087C:RPL19A/YBR084C-A:RPL31A/YDL075W:MRPL1/YDR116C:RPP2B/YDR382W:RPL7A/YGL076C:RPL22A/YLR061W:RPL37A/YLR185W:MRPL24/YMR193W:RPL36A/YMR194W:MRPL44/YMR225C:RPL20A/YMR242C:JJJ1/YNL227C
	cytosolic large ribosomal subunit	10 out of 90 genes, 11.1%	67 out of 4707 background genes, 1.4%	0.00004	0	0	RPL23A/YBL087C:RPL19A/YBR084C-A:RPL31A/YDL075W:RPP2B/YDR382W:RPL7A/YGL076C:RPL22A/YLR061W:RPL37A/YLR185W:RPL36A/YMR194W:RPL20A/YMR242C:JJJ1/YNL227C
	cytosolic part	13 out of 90 genes, 14.4%	157 out of 4707 background genes, 3.3%	0.00068	0	0	RPL23A/YBL087C:RPL19A/YBR084C-A:RPL31A/YDL075W:RPP2B/YDR382W:RPL7A/YGL076C:RPL22A/YLR061W:PEP3/YLR148W:RPL37A/YLR185W:VPS34/YLR240W:RPN13/YLR421C:RPL36A/YMR194W:RPL20A/YMR242C:JJJ1/YNL227C
	cytosol	16 out of 90 genes, 17.8%	285 out of 4707 background genes, 6.1%	0.00775	0	0	RPL23A/YBL087C:RPL19A/YBR084C-A:RPL31A/YDL075W:RPP2B/YDR382W:RPL7A/YGL076C:YJL068C:YNK1/YKL067W:RPL22A/YLR061W:PEP3/YLR148W:RPL37A/YLR185W:VPS34/YLR240W:RPN13/YLR421C:RPL36A/YMR194W:RPL20A/YMR242C:JJJ1/YNL227C:ATX1/YNL259C
k	**vesicle fusion**	5 out of 100 genes, 5.0%	18 out of 4707 background genes, 0.4%	0.00902	0	0	GOS1/YHL031C:PEP3/YLR148W:PEP5/YMR231W:VAM3/YOR106W:SNC2/YOR327C
l	**large ribosomal subunit**	13 out of 100 genes, 13.0%	109 out of 4707 background genes, 2.3%	0.00004	0	0	RPL23A/YBL087C:RPL19A/YBR084C-A:RPL31A/YDL075W:MRPL1/YDR116C:RPP2B/YDR382W:RPL7A/YGL076C:RPL22A/YLR061W:RPL37A/YLR185W:MRPL24/YMR193W:RPL36A/YMR194W:MRPL44/YMR225C:RPL20A/YMR242C:JJJ1/YNL227C
	cytosolic large ribosomal subunit	10 out of 100 genes, 10.0%	67 out of 4707 background genes, 1.4%	0.00011	0	0	RPL23A/YBL087C:RPL19A/YBR084C-A:RPL31A/YDL075W:RPP2B/YDR382W:RPL7A/YGL076C:RPL22A/YLR061W:RPL37A/YLR185W:RPL36A/YMR194W:RPL20A/YMR242C:JJJ1/YNL227C
	cytosolic part	13 out of 100 genes, 13.0%	157 out of 4707 background genes, 3.3%	0.00226	0	0	RPL23A/YBL087C:RPL19A/YBR084C-A:RPL31A/YDL075W:RPP2B/YDR382W:RPL7A/YGL076C:RPL22A/YLR061W:PEP3/YLR148W:RPL37A/YLR185W:VPS34/YLR240W:RPN13/YLR421C:RPL36A/YMR194W:RPL20A/YMR242C:JJJ1/YNL227C
m	**vesicle fusion**	6 out of 150 genes, 4.0%	18 out of 4707 background genes, 0.4%	0.0056	0	0	VAM7/YGL212W:GOS1/YHL031C:PEP3/YLR148W:PEP5/YMR231W:VAM3/YOR106W:SNC2/YOR327C
n	**large ribosomal subunit**	14 out of 150 genes, 9.3%	109 out of 4707 background genes, 2.3%	0.00091	0	0	RPL23A/YBL087C:RPL19A/YBR084C-A:RPL31A/YDL075W:MRPL1/YDR116C:RPP2B/YDR382W:RPL7A/YGL076C:RPL22A/YLR061W:RPL37A/YLR185W:MRPL24/YMR193W:RPL36A/YMR194W:MRPL44/YMR225C:RPL20A/YMR242C:JJJ1/YNL227C:RTC6/YPL183W-A
	cytosolic large ribosomal subunit	10 out of 150 genes, 6.7%	67 out of 4707 background genes, 1.4%	0.00529	0	0	RPL23A/YBL087C:RPL19A/YBR084C-A:RPL31A/YDL075W:RPP2B/YDR382W:RPL7A/YGL076C:RPL22A/YLR061W:RPL37A/YLR185W:RPL36A/YMR194W:RPL20A/YMR242C:JJJ1/YNL227C
o	**structural constituent of ribosome**	20 out of 200 genes, 10.0%	178 out of 4707 background genes, 3.8%	0.0051	0.04	0.04	RPL23A/YBL087C:RPL19A/YBR084C-A:RPL31A/YDL075W:RPL35B/YDL136W:MRPL1/YDR116C:RPP2B/YDR382W:RPL7A/YGL076C:RPL9A/YGL147C:RPL39/YJL189W:RPL22A/YLR061W:RPL37A/YLR185W:RPL38/YLR325C:RPL6B/YLR448W:MRPL24/YMR193W:RPL36A/YMR194W:MRPL44/YMR225C:RPL20A/YMR242C:RPL9B/YNL067W:RPS7A/YOR096W:RTC6/YPL183W-A
p	**cytosolic large ribosomal subunit**	16 out of 200 genes, 8.0%	67 out of 4707 background genes, 1.4%	0.00000	0	0	RPL23A/YBL087C:RPL19A/YBR084C-A:RPL31A/YDL075W:RPL35B/YDL136W:RPP2B/YDR382W:RPL7A/YGL076C:RPL9A/YGL147C:RPL39/YJL189W:RPL22A/YLR061W:RPL37A/YLR185W:RPL38/YLR325C:RPL6B/YLR448W:RPL36A/YMR194W:RPL20A/YMR242C:RPL9B/YNL067W:JJJ1/YNL227C
	large ribosomal subunit	20 out of 200 genes, 10.0%	109 out of 4707 background genes, 2.3%	0.00000	0	0	RPL23A/YBL087C:RPL19A/YBR084C-A:RPL31A/YDL075W:RPL35B/YDL136W:MRPL1/YDR116C:RPP2B/YDR382W:RPL7A/YGL076C:RPL9A/YGL147C:RPL39/YJL189W:RPL22A/YLR061W:RPL37A/YLR185W:RPL38/YLR325C:RPL6B/YLR448W:MRPL24/YMR193W:RPL36A/YMR194W:MRPL44/YMR225C:RPL20A/YMR242C:RPL9B/YNL067W:JJJ1/YNL227C:RTC6/YPL183W-A
	cytosolic part	21 out of 200 genes, 10.5%	157 out of 4707 background genes, 3.3%	0.0003	0	0	RPL23A/YBL087C:RPL19A/YBR084C-A:RPL31A/YDL075W:RPL35B/YDL136W:RPP2B/YDR382W:RPL7A/YGL076C:RPL9A/YGL147C:YGR054W:RPL39/YJL189W:RPL22A/YLR061W:PEP3/YLR148W:RPL37A/YLR185W:VPS34/YLR240W:RPL38/YLR325C:RPN13/YLR421C:RPL6B/YLR448W:RPL36A/YMR194W:RPL20A/YMR242C:RPL9B/YNL067W:JJJ1/YNL227C:RPS7A/YOR096W
	cytosolic ribosome	18 out of 200 genes, 9.0%	130 out of 4707 background genes, 2.8%	0.00103	0	0	RPL23A/YBL087C:RPL19A/YBR084C-A:RPL31A/YDL075W:RPL35B/YDL136W:RPP2B/YDR382W:RPL7A/YGL076C:RPL9A/YGL147C:YGR054W:RPL39/YJL189W:RPL22A/YLR061W:RPL37A/YLR185W:RPL38/YLR325C:RPL6B/YLR448W:RPL36A/YMR194W:RPL20A/YMR242C:RPL9B/YNL067W:JJJ1/YNL227C:RPS7A/YOR096W
	cytosol	27 out of 200 genes, 13.5%	285 out of 4707 background genes, 6.1%	0.00788	0	0	RPL23A/YBL087C:RPL19A/YBR084C-A:RPL31A/YDL075W:RPL35B/YDL136W:RPP2B/YDR382W:RPL7A/YGL076C:RPL9A/YGL147C:YGR054W:YJL068C:RPL39/YJL189W:YNK1/YKL067W:RPL22A/YLR061W:PEP3/YLR148W:RPL37A/YLR185W:VPS34/YLR240W:RPL38/YLR325C:RPN13/YLR421C:RPL6B/YLR448W:RPL36A/YMR194W:RPL20A/YMR242C:RPL9B/YNL067W:JJJ1/YNL227C:ATX1/YNL259C:THI20/YOL055C:RPS7A/YOR096W:YOR302W:VTS1/YOR359W
q	**cytosolic large ribosomal subunit**	17 out of 300 genes, 5.7%	67 out of 4707 background genes, 1.4%	0.00009	0	0	RPL23A/YBL087C:RPL19A/YBR084C-A:REI1/YBR267W:RPL31A/YDL075W:RPL35B/YDL136W:RPP2B/YDR382W:RPL7A/YGL076C:RPL9A/YGL147C:RPL39/YJL189W:RPL22A/YLR061W:RPL37A/YLR185W:RPL38/YLR325C:RPL6B/YLR448W:RPL36A/YMR194W:RPL20A/YMR242C:RPL9B/YNL067W:JJJ1/YNL227C
	large ribosomal subunit	22 out of 300 genes, 7.3%	109 out of 4707 background genes, 2.3%	0.00015	0	0	RPL23A/YBL087C:RPL19A/YBR084C-A:REI1/YBR267W:IMG2/YCR071C:RPL31A/YDL075W:RPL35B/YDL136W:MRPL1/YDR116C:RPP2B/YDR382W:RPL7A/YGL076C:RPL9A/YGL147C:RPL39/YJL189W:RPL22A/YLR061W:RPL37A/YLR185W:RPL38/YLR325C:RPL6B/YLR448W:MRPL24/YMR193W:RPL36A/YMR194W:MRPL44/YMR225C:RPL20A/YMR242C:RPL9B/YNL067W:JJJ1/YNL227C:RTC6/YPL183W-A
	endoplasmic reticulum membrane	19 out of 300 genes, 6.3%	90 out of 4707 background genes, 1.9%	0.00042	0	0	CNE1/YAL058W:RCR1/YBR005W:AGP2/YBR132C:OST4/YDL232W:SUR2/YDR297W:CAX4/YGR036C:VOA1/YGR106C:ICE2/YIL090W:MGA2/YIR033W:STE24/YJR117W:SAC1/YKL212W:ERF2/YLR246W:HMG2/YLR450W:UBX2/YML013W:UBC7/YMR022W:HLJ1/YMR161W:CUE1/YMR264W:OST3/YOR085W:ALG5/YPL227C
	endoplasmic reticulum part	21 out of 300 genes, 7.0%	107 out of 4707 background genes, 2.3%	0.00043	0	0	CNE1/YAL058W:RCR1/YBR005W:AGP2/YBR132C:OST4/YDL232W:SUR2/YDR297W:CAX4/YGR036C:VOA1/YGR106C:ICE2/YIL090W:MGA2/YIR033W:STE24/YJR117W:SAC1/YKL212W:OSH6/YKR003W:ERF2/YLR246W:HMG2/YLR450W:UBX2/YML013W:UBC7/YMR022W:HLJ1/YMR161W:SCJ1/YMR214W:CUE1/YMR264W:OST3/YOR085W:ALG5/YPL227C
	nuclear membrane-endoplasmic reticulum network	19 out of 300 genes, 6.3%	99 out of 4707 background genes, 2.1%	0.00186	0	0	CNE1/YAL058W:RCR1/YBR005W:AGP2/YBR132C:OST4/YDL232W:SUR2/YDR297W:CAX4/YGR036C:VOA1/YGR106C:ICE2/YIL090W:MGA2/YIR033W:STE24/YJR117W:SAC1/YKL212W:ERF2/YLR246W:HMG2/YLR450W:UBX2/YML013W:UBC7/YMR022W:HLJ1/YMR161W:CUE1/YMR264W:OST3/YOR085W:ALG5/YPL227C
	integral to endoplasmic reticulum membrane	9 out of 300 genes, 3.0%	25 out of 4707 background genes, 0.5%	0.00217	0	0	CNE1/YAL058W:RCR1/YBR005W:CAX4/YGR036C:ICE2/YIL090W:STE24/YJR117W:SAC1/YKL212W:ERF2/YLR246W:UBX2/YML013W:CUE1/YMR264W
	intrinsic to endoplasmic reticulum membrane	9 out of 300 genes, 3.0%	25 out of 4707 background genes, 0.5%	0.00217	0	0	CNE1/YAL058W:RCR1/YBR005W:CAX4/YGR036C:ICE2/YIL090W:STE24/YJR117W:SAC1/YKL212W:ERF2/YLR246W:UBX2/YML013W:CUE1/YMR264W

Table 4. (contineued)

r	**cytosolic large ribosomal subunit**	19 out of 400 genes, 4.8%	67 out of 4707 background genes, 1.4%	0.00031	0	0	RPL23A/YBL087C:RPL19A/YBR084C-A:REI1/YBR267W:RPL31A/YDL075W:RPL35B/YDL136W:RPP2B/YDR382W:RPL7A/YGL076C:RPL9A/YGL147C:RPL8A/YHL033C:RPL39/YJL189W:RPL22A/YLR061W:RPL37A/YLR185W:RPL38/YLR325C:RPL6B/YLR448W:RPL36A/YMR194W:RPL20A/YMR242C:RPL9B/YNL067W:JJJ1/YNL227C:RPL20B/YOR312C
	large ribosomal subunit	25 out of 400 genes, 6.2%	109 out of 4707 background genes, 2.3%	0.00056	0	0	RPL23A/YBL087C:RPL19A/YBR084C-A:REI1/YBR267W:IMG2/YCR071C:RPL31A/YDL075W:RPL35B/YDL136W:MRPL1/YDR116C:RPP2B/YDR382W:RPL7A/YGL076C:RPL9A/YGL147C:RPL8A/YHL033C:RPL39/YJL189W:RPL22A/YLR061W:RPL37A/YLR185W:RPL38/YLR325C:RPL6B/YLR448W:MRPL39/YML009C:MRPL24/YMR193W:RPL36A/YMR194W:MRPL44/YMR225C:RPL20A/YMR242C:RPL9B/YNL067W:JJJ1/YNL227C:RPL20B/YOR312C:RTC6/YPL183W-A
	endoplasmic reticulum membrane	21 out of 400 genes, 5.2%	90 out of 4707 background genes, 1.9%	0.00266	0	0	CNE1/YAL058W:RCR1/YBR005W:AGP2/YBR132C:OST4/YDL232W:SUR2/YDR297W:CAX4/YGR036C:VOA1/YGR106C:YTA7/YGR270W:ICE2/YIL090W:MGA2/YIR033W:STE24/YJR117W:SAC1/YKL212W:ERF2/YLR246W:HMG2/YLR450W:UBX2/YML013W:HMG1/YML075C:UBC7/YMR022W:HLJ1/YMR161W:CUE1/YMR264W:OST3/YOR085W:ALG5/YPL227C
	nuclear membrane-endoplasmic reticulum network	22 out of 400 genes, 5.5%	99 out of 4707 background genes, 2.1%	0.0038	0	0	SPO7/YAL009W:CNE1/YAL058W:RCR1/YBR005W:AGP2/YBR132C:OST4/YDL232W:SUR2/YDR297W:CAX4/YGR036C:VOA1/YGR106C:YTA7/YGR270W:ICE2/YIL090W:MGA2/YIR033W:STE24/YJR117W:SAC1/YKL212W:ERF2/YLR246W:HMG2/YLR450W:UBX2/YML013W:HMG1/YML075C:UBC7/YMR022W:HLJ1/YMR161W:CUE1/YMR264W:OST3/YOR085W:ALG5/YPL227C
	endoplasmic reticulum part	23 out of 400 genes, 5.8%	107 out of 4707 background genes, 2.3%	0.00437	0	0	CNE1/YAL058W:RCR1/YBR005W:AGP2/YBR132C:OST4/YDL232W:SUR2/YDR297W:CAX4/YGR036C:VOA1/YGR106C:YTA7/YGR270W:ICE2/YIL090W:MGA2/YIR033W:STE24/YJR117W:SAC1/YKL212W:OSH6/YKR003W:ERF2/YLR246W:HMG2/YLR450W:UBX2/YML013W:HMG1/YML075C:UBC7/YMR022W:HLJ1/YMR161W:SCJ1/YMR214W:CUE1/YMR264W:OST3/YOR085W:ALG5/YPL227C
s	**cytosolic large ribosomal subunit**	25 out of 500 genes, 5.0%	67 out of 4707 background genes, 1.4%	0.00000	0	0	RPL23A/YBL087C:RPL19A/YBR084C-A:REI1/YBR267W:RPL31A/YDL075W:RPL35B/YDL136W:RPP2B/YDR382W:RPL12B/YDR418W:RPL24A/YGL031C:RPL7A/YGL076C:RPL9A/YGL147C:RPL8A/YHL033C:RPL34B/YIL052C:RPL39/YJL189W:RPL40B/YKR094C:RPL8B/YLL045C:RPL22A/YLR061W:RPL37A/YLR185W:RPL38/YLR325C:RPL6B/YLR448W:RPL36A/YMR194W:RPL20A/YMR242C:RPL9B/YNL067W:RPL16B/YNL069C:JJJ1/YNL227C:RPL20B/YOR312C
	large ribosomal subunit	32 out of 500 genes, 6.4%	109 out of 4707 background genes, 2.3%	0.00001	0	0	RPL23A/YBL087C:RPL19A/YBR084C-A:REI1/YBR267W:IMG2/YCR071C:RPL31A/YDL075W:RPL35B/YDL136W:MRPL1/YDR116C:RPP2B/YDR382W:RPL12B/YDR418W:RPL24A/YGL031C:RPL7A/YGL076C:RPL9A/YGL147C:RPL8A/YHL033C:RPL34B/YIL052C:RPL39/YJL189W:RPL40B/YKR094C:RPL8B/YLL045C:RPL22A/YLR061W:RPL37A/YLR185W:RPL38/YLR325C:RPL6B/YLR448W:MRPL39/YML009C:MRPL3/YMR024W:MRPL24/YMR193W:RPL36A/YMR194W:MRPL44/YMR225C:RPL20A/YMR242C:RPL9B/YNL067W:RPL16B/YNL069C:JJJ1/YNL227C:RPL20B/YOR312C:RTC6/YPL183W-A
	endoplasmic reticulum membrane	24 out of 500 genes, 4.8%	90 out of 4707 background genes, 1.9%	0.00282	0	0	CNE1/YAL058W:RCR1/YBR005W:AGP2/YBR132C:OST4/YDL232W:SUR2/YDR297W:CAX4/YGR036C:VMA21/YGR105W:VOA1/YGR106C:YTA7/YGR270W:VMA22/YHR060W:SNL1/YIL016W:ICE2/YIL090W:MGA2/YIR033W:STE24/YJR117W:SAC1/YKL212W:ERF2/YLR246W:HMG2/YLR450W:UBX2/YML013W:HMG1/YML075C:UBC7/YMR022W:HLJ1/YMR161W:CUE1/YMR264W:OST3/YOR085W:ALG5/YPL227C
	nuclear membrane-endoplasmic reticulum network	25 out of 500 genes, 5.0%	99 out of 4707 background genes, 2.1%	0.00522	0	0	SPO7/YAL009W:CNE1/YAL058W:RCR1/YBR005W:AGP2/YBR132C:OST4/YDL232W:SUR2/YDR297W:CAX4/YGR036C:VMA21/YGR105W:VOA1/YGR106C:YTA7/YGR270W:VMA22/YHR060W:SNL1/YIL016W:ICE2/YIL090W:MGA2/YIR033W:STE24/YJR117W:SAC1/YKL212W:ERF2/YLR246W:HMG2/YLR450W:UBX2/YML013W:HMG1/YML075C:UBC7/YMR022W:HLJ1/YMR161W:CUE1/YMR264W:OST3/YOR085W:ALG5/YPL227C
	cytosolic ribosome	30 out of 500 genes, 6.0%	130 out of 4707 background genes, 2.8%	0.00549	0	0	RPL23A/YBL087C:RPL19A/YBR084C-A:REI1/YBR267W:RPL31A/YDL075W:RPL35B/YDL136W:RPP2B/YDR382W:RPL12B/YDR418W:RPL24A/YGL031C:RPL7A/YGL076C:RPL9A/YGL147C:YGR054W:RPL8A/YHL033C:RPL34B/YIL052C:RPL39/YJL189W:RPL40B/YKR094C:RPL8B/YLL045C:RPL22A/YLR061W:RPL37A/YLR185W:MAP1/YLR244C:RPL38/YLR325C:RPL6B/YLR448W:RPL36A/YMR194W:RPL20A/YMR242C:RPL9B/YNL067W:RPL16B/YNL069C:JJJ1/YNL227C:RPS7A/YOR096W:NAT5/YOR253W:RPL20B/YOR312C:RPS6A/YPL090C
	cytosolic part	34 out of 500 genes, 6.8%	157 out of 4707 background genes, 3.3%	0.00666	0	0	RPL23A/YBL087C:RPL19A/YBR084C-A:VPS15/YBR097W:REI1/YBR267W:RPL31A/YDL075W:RPL35B/YDL136W:RPP2B/YDR382W:RPL12B/YDR418W:RPL24A/YGL031C:RPL7A/YGL076C:RPL9A/YGL147C:YGR054W:RPL8A/YHL033C:RPL34B/YIL052C:RPL39/YJL189W:RPL40B/YKR094C:RPL8B/YLL045C:RPL22A/YLR061W:PEP3/YLR148W:RPL37A/YLR185W:VPS34/YLR240W:MAP1/YLR244C:RPL38/YLR325C:RPN13/YLR421C:RPL6B/YLR448W:RPL36A/YMR194W:RPL20A/YMR242C:RPL9B/YNL067W:RPL16B/YNL069C:JJJ1/YNL227C:RPS7A/YOR096W:NAT5/YOR253W:RPL20B/YOR312C:RPS6A/YPL090C
	endoplasmic reticulum part	26 out of 500 genes, 5.2%	107 out of 4707 background genes, 2.3%	0.00743	0	0	CNE1/YAL058W:RCR1/YBR005W:AGP2/YBR132C:OST4/YDL232W:SUR2/YDR297W:CAX4/YGR036C:VMA21/YGR105W:VOA1/YGR106C:YTA7/YGR270W:VMA22/YHR060W:SNL1/YIL016W:ICE2/YIL090W:MGA2/YIR033W:STE24/YJR117W:SAC1/YKL212W:OSH6/YKR003W:ERF2/YLR246W:HMG2/YLR450W:UBX2/YML013W:HMG1/YML075C:UBC7/YMR022W:HLJ1/YMR161W:SCJ1/YMR214W:CUE1/YMR264W:OST3/YOR085W:ALG5/YPL227C

Table 5. The result of Jonckheere-Terpstra test of *his3*Δ *adh6*Δtreated with vanillin.

rank	Parameter	Description	Z value	P value	Q value
1	C13_A	Whole_cell_fitness_for_ellipse	3.55353	3.80E-04	0.087814
2	D130_C	Distance_between_nuclear_brightest_point_in_mother_and_middle_point_of_neck	-3.35427	7.96E-04	0.087814
3	CCV115_A1B	CV_of_Mother_axis_ratio	3.287845	0.00101	0.087814
4	D194_A	Maximal_intensity_of_nuclear_brightness_divided_by_average	3.221424	0.001276	0.087814
5	D108_C	Distance_between_nuclear_gravity_center_in_mother_and_middle_point_of_neck	-3.22142	0.001276	0.087814
6	D112_C	Ratio_of_D108_to_C128	-3.155	0.001605	0.087814
7	D116_C	Distance_between_two_nuclear_gravity_centers_through_middle_point_of_neck	-3.08858	0.002011	0.087814
8	D134_C	Distance_between_two_nuclear_brightest_points_through_middle_point_of_neck	-3.08858	0.002011	0.087814
9	C103_A	Long_axis_length_in_whole_cell	-3.02216	0.00251	0.087814
10	C128_A1B	Distance_between_middle_point_of_neck_and_mother_hip	-3.02216	0.00251	0.087814
11	C12-1_A	Whole_cell_outline_length	-2.95574	0.003119	0.087814
12	DCV155_A	CV_of_Angle_between_C1D2-1_and_C1C1-2	-2.95574	0.003119	0.087814
13	DCV196_A1B	CV_of_Maximal_intensity_of_nuclear_brightness_divided_by_average	-2.95574	0.003119	0.087814
14	C11-1_A	Whole_cell_size	-2.88932	0.003861	0.087814
15	C104_A	Short_axis_length_in_whole_cell	-2.88932	0.003861	0.087814
16	D127_A	Distance_between_nuclear_brightest_point_and_cell_tip	-2.88932	0.003861	0.087814
17	C104_A1B	Short_axis_length_in_mother	-2.88932	0.003861	0.087814
18	C109_A1B	Neck_width	-2.75648	0.005843	0.102691
19	C109_C	Neck_width	-2.75648	0.005843	0.102691
20	D106_C	Ratio_of_D103_to_C103	2.756476	0.005843	0.102691
21	D143_C	Distance_between_nuclear_outline_point_D6-1_in_mother_and_middle_point_of_neck	-2.75648	0.005843	0.102691
22	D196_C	Maximal_intensity_of_nuclear_brightness_divided_by_average_in_whole cell	2.756476	0.005843	0.102691
23	C101_A1B	Whole_cell_size	-2.69006	0.007144	0.106244
24	C115_A1B	Mother_axis_ratio	2.690055	0.007144	0.106244
25	D196_A1B	Maximal_intensity_of_nuclear_brightness_divided_by_average	2.690055	0.007144	0.106244
26	D183_C	Nuclear_axis_ratio_in_bud	-2.69006	0.007144	0.106244
27	A122_A1B	Number_of_bright_actin_patches	-2.62363	0.0087	0.120139
28	C128_C	Distance_between_middle_point_of_neck_and_mother_hip	-2.62363	0.0087	0.120139
29	C11-1_A1B	Mother_cell_size	-2.55721	0.010551	0.123633
30	A9_A1B	Proportion_of_actin_region_at_neck	-2.55721	0.010551	0.123633
31	C13_C	Mother_cell_fitness_for_ellipse	2.557213	0.010551	0.123633
32	D141_C	Distance_between_nuclear_brightest_point_in_mother_and_mother_hip	2.557213	0.010551	0.123633
33	D195_C	Maximal_intensity_of_nuclear_brightness_divided_by_average_in_bud	2.557213	0.010551	0.123633
34	CCV103_A	CV_of_Long_axis_length_in_whole_cell	2.490792	0.012746	0.128902
35	C12-1_A1B	Mother_cell_outline_length	-2.49079	0.012746	0.128902
36	CCV116_C	CV_of_Axis_ratio_ratio	2.490792	0.012746	0.128902
37	ACV102_C	CV_of_Bud_actin_region_ratio_to_total_region	2.490792	0.012746	0.128902
38	ACV122_A	CV_of_Number_of_bright_actin_patches	2.424371	0.015335	0.128902
39	C13_A1B	Mother_cell_fitness_for_ellipse	2.424371	0.015335	0.128902
40	C112_A1B	Distance_between_middle_point_of_neck_and_mother_center	-2.42437	0.015335	0.128902
41	C115_C	Mother_axis_ratio	2.424371	0.015335	0.128902
42	A8-2_C	Total_brightness_of_actin_region_in_bud	-2.42437	0.015335	0.128902
43	A121_C	Maximal_distance_between_patches	-2.42437	0.015335	0.128902
44	D152_C	Mobility_of_nucleus_in_mother	-2.42437	0.015335	0.128902
45	D194_C	Maximal_intensity_of_nuclear_brightness_divided_by_average_in_mother	2.424371	0.015335	0.128902
46	CCV114_C	CV_of_Bud_axis_ratio	2.424371	0.015335	0.128902
47	D125_C	Distance_between_nuclear_gravity_center_in_mother_and_mother_hip	2.35795	0.018376	0.15118
48	A121_A	Maximal_distance_between_patches	-2.29153	0.021933	0.151441
49	D102_A	Distance_between_nuclear_gravity_center_and_mother_tip	-2.29153	0.021933	0.151441
50	CCV115_A	CV_of_Whole_cell_axis_ratio	2.291529	0.021933	0.151441
51	C108_A1B	Short_axis_length_in_bud	-2.29153	0.021933	0.151441
52	C104_C	Short_axis_length_in_mother	-2.29153	0.021933	0.151441
53	A7-2_C	Size_of_actin_region_in_bud	-2.29153	0.021933	0.151441
54	A120_C	Total_length_of_actin_patch_link	-2.29153	0.021933	0.151441
55	D170_C	Angle_between_C4-1D2-1_and_C4-1C1	2.291529	0.021933	0.151441
56	DCV130_C	CV_of_Distance_between_nuclear_brightest_point_in_mother_and_middle_point_of_neck	2.291529	0.021933	0.151441
57	A120_A	Total_length_of_actin_patch_link	-2.22511	0.026074	0.168033
58	C103_A1B	Long_axis_length_in_mother	-2.22511	0.026074	0.168033
59	ACV8-1_A1B	CV_of_Total_brightness_of_actin_region_in_mother	2.225107	0.026074	0.168033
60	ACV123_A1B	CV_of_Ratio_of_actin_patches_to_actin_region	2.225107	0.026074	0.168033
61	CCV126_A	CV_of_Brightness_difference_of_cell_wall	2.158686	0.030875	0.189494
62	D186_C	Total_length_of_two_straight_segments_D12-1C4-1_and_D12-2C4-1	-2.15869	0.030875	0.189494
63	DCV112_C	CV_of_Ratio_of_D108_to_C128	2.158686	0.030875	0.189494

Details of parameters presented are available in SCMD (http://yeast.gi.k.u-tokyo.ac.jp/datamine/).

Table 6. Gene ontology terms detected in the inference result of *his3Δ adh6Δ*.
Each symbol means any enrichment is detected under P value < 0.01 and ND means not detected. Below table shows details of the GO terms.

Rank in the 4718 mutants	*his3Δ adh6Δ*					
	Inference Result			GO term		
	R value	P value	Q value	Process	Function	Component
10	0.585212	6.84E-11	4.87E-09	ND	ND	**a**
20	0.571941	2.27E-10	9.61E-09	**b**	ND	ND
30	0.551621	1.29E-09	3.01E-08	**c**	ND	ND
40	0.541987	2.82E-09	5.11E-08	ND	ND	ND
50	0.525154	1.05E-08	1.56E-07	ND	ND	ND
60	0.510474	3.10E-08	3.82E-07	ND	ND	ND
70	0.503284	5.17E-08	5.63E-07	ND	ND	ND
80	0.497448	7.78E-08	7.57E-07	ND	ND	ND
90	0.489566	1.33E-07	1.16E-06	ND	ND	ND
100	0.486803	1.61E-07	1.29E-06	ND	ND	ND
150	0.466203	6.11E-07	3.45E-06	ND	ND	ND
200	0.437223	3.47E-06	1.44E-05	ND	ND	ND
300	0.399983	2.59E-05	7.41E-05	ND	ND	ND
400	0.371246	1.05E-04	2.26E-04	ND	ND	**d**
500	0.345163	3.33E-04	5.80E-04	ND	ND	ND

	GO_term	Cluster frequency	Background frequency	P-value	FDR	Expected FP	Genes annotated to the term
a	**cytosolic large ribosomal subunit**	3 out of 10 genes, 30.0%	67 out of 4707 background genes, 1.4%	0.00832	0.02	0.02	RPL19A/YBR084C-A:RPP1B/YDL130W:RPL8A/YHL033C
b	**regulation of cell size**	5 out of 20 genes, 25.0%	94 out of 4707 background genes, 2.0%	0.00367	0	0	TEC1/YBR083W:KAP122/YGL016W:FKH1/YIL131C:SFP1/YLR403W:WHI3/YNL197C
	regulation of cellular component size	5 out of 20 genes, 25.0%	102 out of 4707 background genes, 2.2%	0.00544	0	0	TEC1/YBR083W:KAP122/YGL016W:FKH1/YIL131C:SFP1/YLR403W:WHI3/YNL197C
	regulation of anatomical structure size	5 out of 20 genes, 25.0%	102 out of 4707 background genes, 2.2%	0.00544	0	0	TEC1/YBR083W:KAP122/YGL016W:FKH1/YIL131C:SFP1/YLR403W:WHI3/YNL197C
c	**regulation of cell size**	6 out of 30 genes, 20.0%	94 out of 4707 background genes, 2.0%	0.00272	0.06	0.06	TEC1/YBR083W:KAP122/YGL016W:FKH1/YIL131C:BUD8/YLR353W:SFP1/YLR403W:WHI3/YNL197C
	regulation of cellular component size	6 out of 30 genes, 20.0%	102 out of 4707 background genes, 2.2%	0.00435	0.03	0.06	TEC1/YBR083W:KAP122/YGL016W:FKH1/YIL131C:BUD8/YLR353W:SFP1/YLR403W:WHI3/YNL197C
	regulation of anatomical structure size	6 out of 30 genes, 20.0%	102 out of 4707 background genes, 2.2%	0.00435	0.02	0.06	TEC1/YBR083W:KAP122/YGL016W:FKH1/YIL131C:BUD8/YLR353W:SFP1/YLR403W:WHI3/YNL197C
d	**mitochondrion**	107 out of 400 genes, 26.8%	857 out of 4707 background genes, 18.2%	0.00125	0	0	FUN30/YAL019W:CYC3/YAL039C:ERP1/YAR002C-A:PIM1/YBL022C:CBP6/YBR120C:TRX3/YCR083W:SLM3/YDL033C:PUS9/YDL036C:MRP10/YDL045W-A:COX9/YDL067C:CBS1/YDL069C:YDL086W:STF1/YDL130W-A:CRD1/YDL142C:INH1/YDL181W:ARO3/YDR035W:YDR061W:PET100/YDR079W:RSM24/YDR175C:MFB1/YDR219C:LYS4/YDR234W:MRP20/YDR405W:PAD1/YDR538W:RSM18/YER050C:CEM1/YER061C:ERP6/YGL002W:GEP7/YGL057C:NUT1/YGL151W:GCN1/YGL195W:HXK2/YGL253W:MSP1/YGR028W:PIL1/YGR086C:SHY1/YGR112W:YLF2/YHL014C:AIM17/YHL021C:VMR1/YHL035C:CBP2/YHL038C:FYV4/YHR059W:HTD2/YHR067W:MSR1/YHR091C:GEP4/YHR100C:COX23/YHR116W:MSH1/YHR120W:YHR162W:MTG2/YHR168W:YIA6/YIL006W:PKP1/YIL042C:RSM25/YIL093C:POR2/YIL114C:AYR1/YIL124W:REV7/YIL139C:MRS1/YIR021W:MRPL8/YJL063C:MEF2/YJL102W:URA2/YJL130C:YJL147C:QCR8/YJL166W:ATP2/YJR121W:MDM35/YKL053C-A:MRPL31/YKL138C:JEN1/YKL217W:TOS4/YLR183C:LIP2/YLR239C:ECM19/YLR390W:ATP10/YLR393W:FMP27/YLR454W:OGG1/YML060W:ALO1/YML086C:COX14/YML129C:AEP1/YMR064W:MRPS8/YMR158W:COX7/YMR256C:MRP7/YNL005C:COX5A/YNL052W:SUN4/YNL066W:AIM37/YNL100W:LEU4/YNL104C:ESBP6/YNL125C:CPT1/YNL130C:YNL200C:YNL211C:RRG9/YNL213C:MPA43/YNL249C:GOR1/YNL274C:MRPL10/YNL284C:HXT14/YNL318C:CIT1/YNR001C:ATP23/YNR020C:MRPS12/YNR036C:PET494/YNR045W:IFM1/YOL023W:MSE1/YOL033W:PPM2/YOL141W:LIP5/YOR196C:GEP3/YOR205C:AIM41/YOR215C:RDL1/YOR285W:MBF1/YOR298C-A:MSC6/YOR354C:PHR1/YOR386W:AEP3/YPL005W:SYH1/YPL105C:COX11/YPL132W:PET20/YPL159C:RTC6/YPL183W-A:MMT2/YPL224C:ISA2/YPR067W

Table 7. The results of image profiling of the three strains.

Strain	The number of candidate genes（P＜0.05）	The maximum R value	Enrichment ratio of “ribosomal large subunit”
Wild-type (*his3*Δ）	95 genes	0.638	11.9-fold
*erg6*Δ	123 genes	0.653	11.9-fold
*his3*Δ *adh6*Δ	252 genes	0.719	21.4-fold

Table 8. Yeast strains used in this study.

	Strain	Genotype	Souce
BY4741	*his3*Δ	*MAT*a *his3::kanMX leu2 met15 ura3*	EUROSCARF
	*erg6*Δ	*MAT*a *his3 leu2 met15 ura3 erg6::kanMX*	EUROSCARF
	*his3*Δ *adh6*Δ	*MAT*a *his3::kanMX leu2 met15 ura3 adh6::Cg LEU2*	this study

References

Burri, J., Graf, M., Lambelet, P. and Löliger, J. (1989) Vanillin: more than a flavouring agent-a potent antioxidant. *J. Sci. Food Agric.* 48 (1): 49-56

Cantarella M, Cantarella L, Gallifuoco A, Spera A, Alfani F. (2004) Effect of inhibitors released during steam-explosion treatment of poplar wood on subsequent enzymatic hydrolysis and SSF. *Biotechnol Prog.* 20 (1): 200-6.

De Wulf, P. Thonart, P. Gaignage, M. Marlier, A. Paris and M. Paquot, (1986) Bioconversion of vanillin to vanillyl alcohol by Saccharomyces cerevisiae. *Biotechnol. Bioeng. Symp*. 7: 605-616.

Durant S, Karran P. (2003) Vanillins-a novel family of DNA-PK inhibitors. *Nucleic Acids Res.* 31 (19): 5501-12.

Endo A, Nakamura T, Ando A, Tokuyasu K, Shima J. (2008) Genome-wide screening of the genes required for tolerance to vanillin, which is a potential inhibitor of bioethanol fermentation, in Saccharomyces cerevisiae. *Biotechnol Biofuels.* 1 (1): 3.

Endo A, Nakamura T, Shima J. (2009) Involvement of ergosterol in tolerance to vanillin, a potential inhibitor of bioethanol fermentation, in Saccharomyces cerevisiae. *FEMS Microbiol Lett.* 299 (1): 95-9.

E. Rico-Munoz, E.E. Bargiota and P.M. Davidson, (1987) Effect of selected phenolic compounds on the membrane-bound adenosine triphosphatase of Staphylococcus aureus. *Food Microbiol.* 4 (3): 239-249.

Eva Palmqvist1 and Bärbel Hahn-Hägerda (2000) Fermentation of lignocellulosic hydrolysates. II: inhibitors and mechanisms of inhibition. *Bioresource Technology* 74 (1): 25-33

Fei W, Alfaro G, Muthusamy BP, Klaassen Z, Graham TR, Yang H, Beh CT. (2008) Genome-wide analysis of sterol-lipid storage and trafficking in Saccharomyces cerevisiae. *Eukaryot Cell* 7 (2): 401-14.

Fitzgerald DJ, Stratford M, Narbad A. (2003) Analysis of the inhibition of food spoilage yeasts by vanillin. *Int J Food Microbiol.* 86 (1-2): 113-22.

Hahn-Hägerdal B, Galbe M, Gorwa-Grauslund MF, Lidén G, Zacchi G.(2006) Bio-ethanol--the fuel of tomorrow from the residues of today. *Trends Biotechnol.* 24 (12): 549-56.

Hashimoto J, Motohashi K, Sakamoto K, Hashimoto S, Yamanouchi M, Tanaka H, Takahashi T, Takagi M, Shin-ya K. (2009) Screening and evaluation of new inhibitors of hepatic glucose production. *J Antibiot*. 62 (11): 625-9.

Ho K, Yazan LS, Ismail N, Ismail M. (2009) Apoptosis and cell cycle arrest of human colorectal cancer cell line HT-29 induced by vanillin. *Cancer Epidemiol.* 33 (2): 155-60.

Hocking, M.B (1997) Vanillin: synthetic flavoring from spent sulfire liquor. *J. Chem. Ebuc.* 74 (9): 1055-9

Ito H, Fukuda Y, Murata K, Kimura A. (1983) Transformation of intact yeast cells treated with alkali cations. *J Bacteriol.* 153 (1): 163-8.

Jorgensen P, et al. (2002) Systematic identification of pathways that couple cell growth and division in yeast. *Science* 297 (5580): 395-400

Klinke HB, Thomsen AB, Ahring BK. (2004) Inhibition of ethanol-producing yeast and bacteria by degradation products produced during pre-treatment of biomass. *Appl Microbiol Biotechnol.* 66 (1): 10-26

Larroy C, Fernández MR, González E, Parés X, Biosca JA. (2002 a) Characterization of the Saccharomyces cerevisiae YMR318C (ADH6) gene product as a broad specificity NADPH-dependent alcohol dehydrogenase: relevance in aldehyde reduction. *Biochem J.* 361(Pt 1): 163-72.

Larroy C, Parés X, Biosca JA. (2002 b) Characterization of a Saccharomyces cerevisiae NADP(H)-dependent alcohol dehydrogenase (ADHVII), a member of the cinnamyl alcohol dehydrogenase family. *Eur J Biochem.* 269 (22): 5738-45.

Liang JA, Wu SL, Lo HY, Hsiang CY, Ho TY. (2009) Vanillin inhibits matrix metalloproteinase-9 expression through down-regulation of nuclear factor-kappaB signaling pathway in human hepatocellular carcinoma cells. *Mol Pharmacol.* 75 (1): 151-7.

Markovich S, Yekutiel A, Shalit I, Shadkchan Y, Osherov N. (2004) Genomic approach to identification of mutations affecting caspofungin susceptibility in Saccharomyces cerevisiae. *Antimicrob Agents Chemother.* 48 (10): 3871-6.

Ohnuki S, Oka S, Nogami S, Ohya Y. (2010) High-content, image-based screening for drug targets in yeast. *PLoS One.* 5 (4): e10177.

Ohtani M, Saka A, Sano F, Ohya Y, Morishita S 2004 Development of image processing program for yeast cell morphology. *J Bioinform Comput Biol.* 1 (4): 695-709.

Ohya Y, Sese J, Yukawa M, Sano F, Nakatani Y, Saito TL, Saka A, Fukuda T, Ishihara S, Oka S, Suzuki G, Watanabe M, Hirata A, Ohtani M, Sawai H, Fraysse N, Latgé JP, François JM, Aebi M, Tanaka S, Muramatsu S, Araki H, Sonoike K, Nogami S, Morishita S (2005) High-dimensional and large-scale phenotyping of yeast mutants. *Proc Natl Acad Sci U S A*. 102 (52): 19015-20.

Parawira W, Tekere M. (2010) Biotechnological strategies to overcome inhibitors in lignocellulose hydrolysates for ethanol production: review.*Crit Rev Biotechnol*. 1-12 early online.

Petersson A, Almeida JR, Modig T, Karhumaa K, Hahn-Hägerdal B, Gorwa-Grauslund MF, Lidén G. (2006) A 5-hydroxymethyl furfural reducing enzyme encoded by the Saccharomyces cerevisiae ADH6 gene conveys HMF tolerance. *Yeast* 23 (6): 455-64.

Saito, T.L., Ohtani, M., Sawai, H., Sano, F., Saka, A., Watanabe, D., Yukawa, M., Ohya, Y., and Morishita, S. (2004) SCMD:Saccaromyces cerevisiae morphological database. *Nuc. Acid Res*. 32: D319-22.

Wendakoon and M. Sakaguchi, (1995) Inhibition of amino acid decarboxylase activity of Enterobacter aerogenes by active components of spices. *J. Food Prot.* 58 (3): 280-283.

Yunqiao Pu, Dongcheng Zhang, Preet M. Singh, Arthur J. Ragauskas. (2008) The new forestry biofuels sector. Biofuels, *Bioproducts and Biorefining*. 2 (1): 58-73